Higher Order Method of Moments for Current Flow Modelling of Sector Shaped Conductors and Scattering by Dielectric Cylinder

by

Mohammad Shakander Hosen

A Thesis Submitted to the Faculty of Graduate Studies of

The University of Manitoba

in partial fulfilment of the requirements of the degree of

MASTER OF SCIENCE

Department of Electrical and Computer Engineering
University of Manitoba
Winnipeg, Manitoba, Canada

Abstract

Design of complex multi conductor transmission lines (MTLs) depends on the knowledge of per unit length (p.u.l.) inductance and resistance along with p.u.l. capacitance and conductance. In order to calculate with controlled precision p.u.l. inductance and resistance of complex MTLs of arbitrary cross-section higher order numerical methods are required. Such method based on Higher Order (HO) Method of Moment (MoM) solution of Surface Volume Surface Electric Field Integral Equation (SVS-EFIE) is proposed in this thesis. The cross-section of the MTLs is discretized with higher order quadrilateral elements to reduce the error associated with the geometry representation. The unknown currents are approximated by high order polynomial basis functions for accurate representation of their sophisticated behaviour according to the skin- and proximity-effects. Memory requirement for the proposed method is shown to be substantially smaller than that of the HO Finite Element Method (FEM) due to discretization of only the MTLs cross-section and not the surrounding volume. Analogous SVS-EFIE is shown in the thesis to be solved with HO-MoM to calculate the scattered field with high accuracy inside 2-D dielectric scatterers of arbitrary shape under TM-polarization.Various obstacles in achieving error controlled HO-MoM solution of SVS-EFIE are overcome in this thesis. In order to get error controlled solution of the sought fields, singularity extraction is performed on 1-D and 2-D HO elements when calculating the integrals related to HO-MoM discretization. As the HO FEM must truncate its mesh within a certain region around the object of interest in order to perform one-to-one comparison of the fields computed using the HO-MoM solution of the SVS-EFIE against HO-FEM the same region of interest must be considered. In this work a grounded cylindrical cavity of large radius surrounding MTLs is introduced for truncation of the FEM mesh. To enforce the same boundary condition in the HO-MoM solution the Green's function of the cylindrical cavity is analytically derived and used in the SVS-EFIE formulation.

Author's Publications

The author has co-authored in these following publications towards the M.Sc. degree

- F. Sheikh Hosseini Lori, **M. S. Hosen**, A. Menshov, M. Shafieipour, and V.Okhmatovski, "New Higher-Order Method of Moments for Accurate Inductance Extraction in Transmission Lines of Complex Cross-Sections," *IEEE Transactions on Microwave Theory and Techniques*, vol. 65, pp. 5104-5112, 2017.

- F. Sheikh Hosseini Lori, **M. S. Hosen**, V.Okhmatovski, "Higher Order MoM Solution of the New Single-Source Surface Integral Equation for 2D TM and TE Scattering by Dielectric Cylinder," *IEEE Transactions on Microwave Theory and Techniques (Submitted).*

- F. Sheikh Hosseini Lori, **M. S. Hosen**, and V. Okhmatovski, "Higher Order Method of Moments Solution of the New Vector Single-Source Surface Integral Equation for 2D TE Scattering by Dielectric Objects," *2017 IEEE MTT-S Intl. Conf. on Numerical Electromagnetic and Multiphysics Modelling and Optimization (NEMO),* Sevilla, Spain.

- F. Sheikh Hosseini Lori, **M. S. Hosen**, A. Menshov, M. Shafieipour, and V. Okhmatovski, "Accurate Transmission Lines Characterization via Higher Order Moment Method Solution of Novel Single-Source Integral Equation," *2017 IEEE MTT-S Intl. Microwave Symp.,* Hawaii, USA.

- F. Sheikh Hosseini Lori, **M. S. Hosen**, A. Menshov, M. Shafieipour, and V. Okhmatovski, "Accurate Characterization of Coaxial Transmission Line via Higher Order Moment Method Solution of Novel Single-Source Surface Integral Equation," *2017 IEEE Workshop on Signal and Power Integrity,* Baveno, Italy.

Contributions

The authors contribution included in this thesis was to get an error controlled HO-MoM solution of Single-Source SVS-EFIE for scalar TM case for sector shaped MTLs by using Lagrangian type interpolation based geometry discretization and applying singularity extraction method on HO 1-D element.

Acknowledgments

The dream begins with a teacher who believes in you, who tugs and pushes and leads you to the next plateau, sometimes poking you with a sharp stick called "truth."–Dan Rather(October 31, 1931)

There are a few professors in the world who can make a student discover his true potential, undoubtably my supervisor Professor Vladimir Okhmatovski is one of them. I am grateful to him because of his knowledge, wisdom and skill which he has been bestowing upon me for last two years. Thanks for his patience and inspiration which let me grow. I believe his teachings will guide and accompany me for the rest of my life. This work wouldn't have been possible without his support and guidance.

Special thanks to Dr. F. Sheikh Hosseini Lori, Reza Golami, Anton Menshov, and Dr. Mohammad Shafieipour for supporting me throughout the whole program. Without their support life would've been harder.

I would like to show my gratitude to examining committee members Professor Behzad Kordi and Dr. Mohammad Shafieipour for evaluation of this work and their valuable comments.

Thanks and gratitude to the Natural Sciences and Engineering Research Council of Canada, University of Manitoba, and University of Manitoba Graduate Students Association for financial support to complete my research.

I can't thank enough my parents who were there whenever i needed them. Finally, I would like to thank my friends for their support and inspiring words.

The strength of a nation derives from the integrity of the home.
–Confucius (551 BC - 479 BC)

Dedicated to my parents Shirin Aktar and Zakir Hussain, my sisters Tahmina and Tasu and my nieces Mim and Mahnoor.

Table of Contents

List of Tables

List of Figures

Notation, Symbols and Acronyms

Most commonly used symbols and notations in this thesis are listed below

- **Vector representation:** are represented by bold letters such as electric field is $\boldsymbol{E}$, and magnetic field is $\boldsymbol{H}$.
- **Scalar integral operators:** are denoted by upper-case calligraphic letters such as $\mathcal{T}$.
- **Scalar matrices:** are denoted by upper-case calligraphic letters such as Z.
- **Spatial derivative operators:** spatial gradient, divergence, and curl operators are given as $(\boldsymbol{\nabla})$,$(\boldsymbol{\nabla}\cdot)$ and $(\boldsymbol{\nabla}\times)$.

Table 0.1: Common Symbols and Notations

Symbol	Description
$\hat{\mathbf{x}}$, $\hat{\mathbf{y}}$, $\hat{\mathbf{z}}$	Unit vectors in the x, y and z directions.
$\hat{\mathbf{n}}$	Normal unit vector outward to the boundary.
$\hat{\mathbf{t}}$	Tangential unit vector to the boundary.
$\boldsymbol{r}$, $\boldsymbol{r}'$	Position vectors in the 3-D Cartesian coordinate system.
$\boldsymbol{\rho}$, $\boldsymbol{\rho}'$	Position vectors in the 2-D Cartesian coordinate system.
ϵ_0	Permittivity of free-space.
ϵ	Relative complex permittivity of the scatterer.
σ	Conductivity of the scatterer.
μ_0	Permeability of free-space.

μ_r	Relative permeability of the scatterer.
k_0	Wavenumber of free-space.
k_ϵ	Wavenumber inside the scatterer.
ω	Radial frequency.
f	Frequency of operation.
$\mathtt{t}$	Time variable.
λ	Wavelength.
Γ	Gram matrix.
$\boldsymbol{E}^{\text{inc}}$	Time-harmonic incident electric-field for a transmitter.
$\boldsymbol{H}^{\text{inc}}$	Time-harmonic incident magnetic-field for a transmitter.
$\boldsymbol{E}^{\text{scat}}$	Time-harmonic scattered electric-field.
$\boldsymbol{E}$	Time-harmonic total electric-field.
$\boldsymbol{j}$	Polarization current density.
$\boldsymbol{J}$	Fictitious SVS surface source density.
Ψ	The highest order of 2-D basis function.
Ω	The highest order of 1-D basis function.
∂S	Boundary of the 2-D object.
S	Surface of the 2-D object.
∂V	Boundary of the 3-D object.
V	Volume of the 3-D object.
ℓ	Length variable.
Re	Real part operator.
Im	Imaginary part operator.
$\boldsymbol{\nabla}$	Gradient operator.
$\boldsymbol{\nabla}\cdot$	Divergence operator.
$\boldsymbol{\nabla}\times$	Curl operator.
$\boldsymbol{\nabla}\times\boldsymbol{\nabla}\times$	Curl curl operator.
∇^2	The Laplacian.
$(\cdot)^{-1}$	Inverse operator.
$\langle\cdot\,,\cdot\rangle$	Inner product.

Acronym	Description
EM	Electromagnetic
BC	Boundary Condition
CEM	Computational Electromagnetic
CAD	Computer Aid Design
IE	Integral Equation
MoM	Method of Moments
LO	Low Order
HO	Higher Order
HO-MoM	Higher Order Method of Moments
FEM	Finite Element Method
FDM	Finite Difference Method
HO-FEM	Higher Order Finite Element Method
SVS-IE	Surface Volume Surface Integral Equation
SIE	Surface Integral Equation
SSIE	Single Source Surface Integral Equation
VIE	Volume Integral Equation
V-EFIE	Volume Electric Field Integral Equation
PEC	Perfect Electric Conductor
EFIE	Electric Field Integral Equation
SVS-EFIE	Surface Volume Surface Electric Field Integral Equation
MFIE	Magnetic Field Integral Equation
TM	Transverse Magnetic Field Mode
TEM	Transverse Electro Magnetic Mode
TE	Transverse Electric Field Mode
MTLs	Multi Conductor Transmission Lines
SLAEs	System of Linear Algebraic Equations

1

Introduction

Who is wise? He that learns from everyone.
Who is powerful? He that governs his passion.
Who is rich? He that is content.
Who is that? Nobody.–Benjamin Franklin(1706-1790)

1.1 Motivation and Current State of the Art

In order to build MTL model it is required to know p.u.l. inductance, resistance, capacitance and conductance beforehand [1–3]. It is practical to create virtual model of MTL and perform electromagnetic transient (EMT) simulation [4]. Virtual prototyping can be made cost efficient and reliable. Different kinds of electromagnetic solvers can be used to gain these parameters such as partial differential equation based FEM [5] or Finite Difference Method (FDM) [6] solvers and integral equation [7, 8] based MoM [9] solvers. FEM solves partial differential equation with a boundary condition to find the unknown field quantity inside or outside an object of interest [6]. The drawback of FEM is that one needs to discretize the domain outside the object of interest and impose boundary condition to truncate the mesh. The advantage of the

FEM is that it is well suited for modelling inhomogeneous materials and geometrically complex objects [5]. The alternative to the FEM is the method of integral equations. Commonly used integral equations of electromagnetics are the Electric Field Integral Equation (EFIE) [7], Magnetic Field Integral Equation (MFIE) [7], Combined Field Integral Equation (CFIE) [10], Poggio-Miller-Chang- Harrington-Wu-Tsai (PMCHWT) formulation [11] [12], Müller formulation [13] and Volume Integral Equation (VIE) [14]. Surface Integral Equations (SIE) for Perfect Electric Conductors (PEC) [7] like EFIE and MFIE represent the unknown field quantity with equivalent electric and magnetic surface currents through surface equivalence principle [15] and enforcing boundary conditions [7] on tangential electric and magnetic field. The number of unknowns is typically much smaller for SIE compared to FEM because this kind of formulation discretizes only the surface of the object not the whole volume [16].

The EFIE can handle both open and closed structure but has low frequency breakdown [17]. This problem can be handled by using Augmented EFIE (A-EFIE) [18] which uses electric charge as an extra unknown. The MFIE is not applicable for analysis of open structures [7] and also has low frequency breakdown like EFIE. Additionally, both EFIE and MFIE exhibit interior spurious resonances when applied on closed structures. Hence, their solutions may not be unique at certain irregular frequencies [7]. To solve this problem EFIE and MFIE can be linearly combined to formulate new integral equation called CFIE [19]. The CFIE provides unique solution at every frequency but isn't applicable to open structures and also suffers from the low-frequency and oversampling breakdowns.

The VIE, on the other hand, is free of spurious resonances as well as the low-frequency and overdiscretization breakdowns. Solving VIE is computationally expensive, however, because it discretizes the whole volume of the object [14]. As a result number of unknowns is relatively high but this formulation is well suited for inhomogeneous objects [14].

Instead of solving unknown throughout the whole volume, electric field for each observation point inside the object can be calculated with superposition of fields contributed by all the point sources in the boundary. This enables formulations of a new kind of single source surface integral equation formulation termed SVS-EFIE [25].

In this IE formulation the unknowns are on the surface of the object. Which means it has less number of unknowns in comparison to V-EFIE. SVS-EFIE is formulated by using only EFIE type Green's function which makes it easily combined with the multi layered media Green's function for analysis of under ground MTLs [50]. The SVS-EFIE can be accelerated by fast algorithms such as Multi Level Fast Multipole Method (MLFMA) [65], Fast Fourier Transform (FFT) based methods [63, 64] etc. But SVS-EFIE has some drawbacks too. It has three different operators (surface to surface, surface to volume, and volume to surface) [25]. Hence, one must discretize both cross-section and boundary of the object which requires additional memory and CPU time. As a result, its numerical solution is computationally expensive when obtained directly without aid of fast algorithms.

Previously, SVS-EFIE was solved with Lower Order (LO) MoM for p.u.l. resistance and inductance extraction [25]. When doing EMT simulation on MTLs it is well known fact that with the change of frequency, p.u.l. inductance and capacitance doesn't change that much but p.u.l. resistance changes quite a lot. And its observed that at higher frequencies resistive term of impedance $Z = R + i\omega L$ can be orders magnitude lower than the inductive term [2]. So in order to capture the p.u.l. resistance correctly within desired error SVS-EFIE must be solved with a method like HO-MoM.

1.2 Thesis Research Scope

The overall goal of this thesis is to explore HO-MoM solution of recently developed SVS-EFIE [25] for current flow model and scattering from the objects of arbitrary shape in TM mode.

In Chapter 2 detailed derivation of SVS-EFIE from VIE is shown for a single conductor in TM mode under magneto quasi static approximation.

HO-MoM solution of SVS-EFIE for p.u.l. inductance and resistance extraction in TM mode under magneto quasi static approximation for sector shaped MTL is presented in Chapter 3.

Chapter 4 discusses HO-MoM solution of SVS-EFIE for full wave scattering and

radiation problem of 2-D non-magnetic homogeneous dielectric scatterers of arbitrary cross-sections.

Chapter 5 analyzes various challenges which were encountered in this work towards achievement of error controlled solution of SVS-EFIE. It emphasizes the method for singularity extraction on 1-D HO elements, derivation of Green's function of cylindrical cavity necessary for comparing results obtained by HO-MoM solver with HO-FEM based solver, and the study of skin effect in current flow in a circular conductor at high frequencies.

Finally Chapter 6 summarizes the whole thesis and mentions about the future works related to this thesis.

2

Surface-Volume-Surface Integral Equation (SVS-EFIE)

2.1 Maxwell's Equations

Time domain Maxwell's equations can be expressed as follows:

$$\boldsymbol{\nabla} \times \boldsymbol{E}(\boldsymbol{r}, t) = -\frac{\partial}{\partial t}\boldsymbol{B}(\boldsymbol{r}, t), \tag{2.1}$$

$$\boldsymbol{\nabla} \times \boldsymbol{H}(\boldsymbol{r}, t) = \frac{\partial}{\partial t}\boldsymbol{D}(\boldsymbol{r}, t) + \boldsymbol{j}(\boldsymbol{r}, t), \tag{2.2}$$

$$\boldsymbol{\nabla} \cdot \boldsymbol{D}(\boldsymbol{r}, t) = \rho(\boldsymbol{r}, t), \tag{2.3}$$

$$\boldsymbol{\nabla} \cdot \boldsymbol{B}(\boldsymbol{r}, t) = 0, \tag{2.4}$$

where $\boldsymbol{E}$ is the electric field, $\boldsymbol{H}$ is the magnetic field, $\boldsymbol{D}$ is the electric flux density, $\boldsymbol{B}$ is the magnetic flux density, $\boldsymbol{j}$ is the volume electric current density and ρ is the electric charge density. Before Maxwell Ampere's law had this following form

$$\boldsymbol{\nabla} \times \boldsymbol{H}(\boldsymbol{r}, t) = \boldsymbol{j}(\boldsymbol{r}, t). \tag{2.5}$$

The problem with (2.5) is that if we take divergence of this equation it becomes $\boldsymbol{\nabla} \cdot \boldsymbol{j}(\boldsymbol{r}, t) = 0$ because divergence of curl is zero. The question then is whether

$\boldsymbol{\nabla} \cdot \boldsymbol{j}(\boldsymbol{r}, t)$ is always zero or not. We are going to take a look at current flowing through a capacitor when a time varying voltage source is applied. In this case we know that the condition $\boldsymbol{\nabla} \cdot \boldsymbol{j}(\boldsymbol{r}, t) = 0$ is not true since there is no charge between the plates of the capacitor. Then why do we have a current flow through capacitor? To answer this question we have to go to Maxwell's explanation. Maxwell knew from Faraday that time varying magnetic field creates electric field and from that he came up with the idea that changed the world forever. He said that time varying electric field also creates magnetic field. Now we can explain how the current flow is happening through capacitor. The current is related to the change of electric flux in the capacitor. So Maxwell called this current the displacement current, $\boldsymbol{j}_d(\boldsymbol{r}, t) = \frac{\partial}{\partial t}\boldsymbol{D}(\boldsymbol{r}, t)$. By adding this term in Ampere's law, Maxwell unified all four laws of Electromagnetism. From Maxwell we knew that although there is no charge in vacuum but time varying electric field and magnetic field creates each other. Because of this phenomena electromagnetic wave such as light can travel through perfect vacuum [26].

2.2 Volume Integral Equation (VIE)

Since magnetic flux vector $\boldsymbol{B}$ is solenoidal, we can represent $\boldsymbol{B}$ as curl of an auxiliary vector potential as

$$\boldsymbol{B} = \boldsymbol{\nabla} \times \boldsymbol{A}, \tag{2.6}$$

where $\boldsymbol{A}$ is the magnetic vector potential. Another logic behind representing magnetic flux like this is, it also satisfies Gauss law $\boldsymbol{\nabla} \cdot \boldsymbol{B} = 0$ cause $\boldsymbol{\nabla} \cdot \boldsymbol{\nabla} \times \boldsymbol{A} = 0$. If we substitute $\boldsymbol{B}$ (2.6) into Faradays law in frequency domain $\boldsymbol{\nabla} \times \boldsymbol{E} = -i\omega\boldsymbol{B}$, then we have [27]

$$\boldsymbol{\nabla} \times (\boldsymbol{E} + i\omega\boldsymbol{A}) = 0. \tag{2.7}$$

Since $(\boldsymbol{E} + i\omega\boldsymbol{A})$ is a conservative field so it can be represented as negative of $\boldsymbol{\nabla}\phi$ where ϕ is the scalar potential as

$$\boldsymbol{\nabla} \times (\boldsymbol{E} + i\omega\boldsymbol{A}) = \boldsymbol{\nabla} \times (-\boldsymbol{\nabla}\phi). \tag{2.8}$$

If we integrate (2.8) then electric field can be represented in terms of vector and scalar potential as follows [27]

$$\boldsymbol{E} = -i\omega\boldsymbol{A} - \boldsymbol{\nabla}\phi. \tag{2.9}$$

Under magneto quasi static approximation (i.e. when $\sigma >> \omega\epsilon_0$ where σ is the conductivity and ϵ_0 is the free space permittivity), inside the conductor medium we can neglect displacement current $\boldsymbol{j}_d = j\omega\epsilon_0\boldsymbol{E}$ because it is much smaller than volume current of conductivity $\boldsymbol{j} = \sigma\boldsymbol{E}$ [20]. Under this particular condition if we substitute $\boldsymbol{B}$ (2.6) into Ampere's Law in frequency domain we get

$$\boldsymbol{\nabla} \times \mu_0\boldsymbol{H} = \boldsymbol{\nabla} \times \boldsymbol{\nabla} \times \boldsymbol{A} = \mu_0\boldsymbol{j}, \tag{2.10}$$

where μ_0 is the free space permeability. If we use vector identity $\boldsymbol{\nabla} \times \boldsymbol{\nabla} \times \boldsymbol{A} = \boldsymbol{\nabla}(\boldsymbol{\nabla} \cdot \boldsymbol{A}) - \nabla^2\boldsymbol{A}$ and Coulomb gauge $\boldsymbol{\nabla} \cdot \boldsymbol{A} = 0$ in (2.10), it gives us vector form of Poisson's equation as

$$\nabla^2\boldsymbol{A} = -\mu_0\boldsymbol{j}. \tag{2.11}$$

For 2-D conducting media if we assume that volumetric current is flowing only in z direction so $\boldsymbol{j} = j_z \cdot \hat{\mathbf{z}}$. We know that $\boldsymbol{j}$ and $\boldsymbol{A}$ are co-linear which makes $\boldsymbol{A} = A_z \cdot \hat{\mathbf{z}}$. Now we can write scalar Poisson's equation for A_z as

$$\nabla^2 A_z = -\mu_0 j_z. \tag{2.12}$$

In free space the conductivity σ is zero , and the vector potential created by a filament of current (i.e. point source $\mu_0 j_z = \mu_0 I\delta(\boldsymbol{\rho} - \boldsymbol{\rho})$) with magnitude $\mu_0 I = 1\text{A} \cdot \text{H/m}$) satisfies following Poisson equation

$$\nabla^2 G_0(\boldsymbol{\rho}, \boldsymbol{\rho}') = -\delta(\boldsymbol{\rho} - \boldsymbol{\rho}'), \tag{2.13}$$

where

$$G_0(\boldsymbol{\rho}, \boldsymbol{\rho}') = -\frac{1}{2\pi}\ln(|\boldsymbol{\rho} - \boldsymbol{\rho}'|) \tag{2.14}$$

is the free space Green's function. Now we will represent A_z with convolution of

Green's function and volumetric current distribution as follows

$$A_z(\boldsymbol{\rho}) = \mu_0 \int_V j_z(\boldsymbol{\rho}')G_0(\boldsymbol{\rho}, \boldsymbol{\rho}')dv', \tag{2.15}$$

where V is the volume of the conducting media. For a 2-D conductor if we assume that scalar potential ϕ is only changing in z direction equation (2.9) becomes

$$E_z + i\omega A_z = -\frac{d\phi}{dz}. \tag{2.16}$$

According to Ohm's law [20] volumetric current and electric field inside conductor media follows this relationship

$$j_z = \sigma E_z. \tag{2.17}$$

For a 2-D conductor with cross sectional area S if we substitute j_z from (2.17) into (2.15) we get A_z as

$$A_z(\boldsymbol{\rho}) = \sigma\mu_0 \int_S E_z(\boldsymbol{\rho}')G_0(\boldsymbol{\rho}, \boldsymbol{\rho}')ds';\ \boldsymbol{\rho} \in S. \tag{2.18}$$

At this moment we will plugin A_z into equation (2.16) and it will turn into VIE for 2-D conductor for unknown E_z as follows

$$E_z(\boldsymbol{\rho}) + i\omega\mu_0\sigma \int_S E_z(\boldsymbol{\rho}')G_0(\boldsymbol{\rho}, \boldsymbol{\rho}')ds' = V_{\text{p.u.l.}};\ \boldsymbol{\rho} \in S, \tag{2.19}$$

where $V_{\text{p.u.l.}} = -\frac{d\phi(z)}{dz}$ is the voltage drop per unit length. Same VIE can be written by using Ohm's law (2.17) when the unknown is volumetric current j_z as

$$\frac{j_z(\boldsymbol{\rho})}{\sigma} + i\omega\mu_0 \int_S j_z(\boldsymbol{\rho}')G_0(\boldsymbol{\rho}, \boldsymbol{\rho}')ds' = V_{\text{p.u.l.}};\ \boldsymbol{\rho} \in S. \tag{2.20}$$

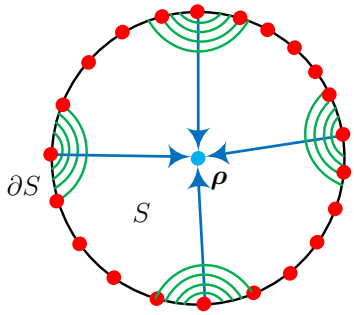

Figure 2.1: Single circular conductor with cross section S and boundary ∂S.

2.3 Surface-Volume-Surface Integral Equation (SVS-EFIE) via Volume Integral Equation (VIE)

Electric field E_z for each observation point $\boldsymbol{\rho}$ inside the object can be calculated with superposition of fields contributed by all the point sources in the boundary ∂S demonstrated in Fig. 2.1 as [25]

$$E_z(\boldsymbol{\rho}) = -i\omega\mu_0 \int_{\partial S} J_z(\boldsymbol{\rho}')G_\sigma(\boldsymbol{\rho},\boldsymbol{\rho}')d\boldsymbol{\rho}'; \boldsymbol{\rho} \in S, \tag{2.21}$$

where J_z is the unknown surface weighting function, $G_\sigma(\boldsymbol{\rho},\boldsymbol{\rho}') = \frac{1}{4i}H_0^{(2)}(k_\sigma|\boldsymbol{\rho}-\boldsymbol{\rho}'|)$ is the Green's function of the conductor media and, $H_0^{(2)}$ is the Hankel function of second kind and of zeroth order. We know that for source points on the boundary $\boldsymbol{\rho}' \in \partial S$ the Green's function G_σ satisfies the Helmholtz equation for all the observation points inside the conductor excluding boundary as

$$\nabla^2 G_\sigma(\boldsymbol{\rho},\boldsymbol{\rho}') + k_\sigma^2 G_\sigma(\boldsymbol{\rho},\boldsymbol{\rho}') = 0, \quad \boldsymbol{\rho} \in S. \tag{2.22}$$

Since G_σ satisfies homogenous Helmholtz equation, superposition of G_σ with some weighting function J_z will also satisfy the same equation. That means E_z, constructed as superposition of waves G_σ (2.21), satisfies the same homogeneous Helmholtz equation as

$$\nabla^2 E_z(\boldsymbol{\rho}) + k_\sigma^2 E_z(\boldsymbol{\rho}) = 0, \quad \boldsymbol{\rho} \in S, \tag{2.23}$$

where $k_\sigma = \sqrt{\frac{\omega\mu\sigma}{2}}(1-i)$ is the complex wave number of the conductor media. Now we will plugin E_z from (2.21) into VIE (2.19) and constrain the latter at the boundary ∂S instead of the cross-section S. This substitution produces scalar SVS EFIE [25] for TM case for a single conductor shown in Fig. 2.1 as following

$$-i\omega\mu_0 \int_{\partial S} J_z(\boldsymbol{\rho}')G_\sigma(\boldsymbol{\rho},\boldsymbol{\rho}')d\boldsymbol{\rho}' - \sigma(\omega\mu_0)^2 \int_{\partial S}\left[\int_S G_0(\boldsymbol{\rho},\boldsymbol{\rho}')G_\sigma(\boldsymbol{\rho},\boldsymbol{\rho}'')ds'\right]\times J_z(\boldsymbol{\rho}'')d\boldsymbol{\rho}'' = V_{\text{p.u.l.}}\ ;\quad \boldsymbol{\rho}\in\partial S. \quad (2.24)$$

The SVS EFIE (2.24) is a single source surface integral equation for which the unknown quantity is fictitious surface current density J_z. Once we compute the surface current density J_z we can also construct volumetric current density j_z. In this Chapter SVS EFIE has been derived for a single conductor. In the next Chapter we will derive and solve SVS EFIE with HO-MoM for extracting p.u.l. resistance and inductance for a sector shaped MTLs.

3

Higher Order Method of Moments for Current Flow Modelling of Sector Shaped MTLs

3.1 Introduction

Electro Magnetic Transient (EMT) simulation of MTLs requires extraction of p.u.l. resistance R, inductance L, capacitance C, and conductance G matrices. These matrices are feed into Telegraphers Equations for determining transient behaviour of currents and voltages in the MTLs. Time domain analysis of MTLs can be done by doing inverse Fourier transform after performing the frequency domain analysis or directly through numerical integration of the Telegraphers Equaitons [21]. The p.u.l. conductance and capacitance matrices are calculated by solving equivalent electrostatic problem [20]. The p.u.l. inductance and resistance matrices are calculated by solving equivalent magnetostatic problem. One way to obtain these matrices is to solve quasi magnetostatic formulation of SVS-EFIE [25] for Quasi-Transverse-Magnetic (TM) mode. To solve SVS-EFIE using method of moments [7, 9] first we need to model the geometry of the object and define position vectors by using polynomial interpolation based on Lagrange [60], Legendre [61], or other polynomials. Subsequently, we have to discretize the unknown surface and volumetric current den-

sity with appropriate basis functions and then test the SVS-EFIE with appropriate test functions.These basis and test functions can be created using monomials, Lagrange, Legendre, or other types of polynomials [67]. This process of discretizing the currents and testing the equation produces a System of Linear Algebraic Equations (SLAEs) with respect to unknown coefficients of surface current density. Once we find these unknown coefficients they can be used to calculate the unknown surface current density as well as volume current density [25].

To solve SVS-EFIE with lower order MoM, we use first order elements such as straight lines to represent the boundary and planar quadrilaterals to represent the 2-D cross section. The unknown surface and volume current densities are expanded over the zero-th order pulse basis functions [25].

To solve SVS-EFIE with higher order MoM we represent the geometry of the object of interest by discretizing it with higher order curved elements on the boundary and curved quadrilateral in the cross section for 2-D case. The unknown surface and volume current densities with higher order polynomials [47]. HO-MoM solution of SVS-EFIE was formulated for any arbitrary number of conductors [59]. In this Chapter we will formulate SVS-EFIE for extracting p.u.l. resistance and inductance matrices in 5 conductor sectorial cable.

3.2 Derivation of SVS-EFIE for Current Flow Modelling of Sector Shaped MTLs

Consider a sectorial cable which consists of 4 sector shaped core conductors and a sheath with cross-section termed as S^{γ} and boundary ∂S^{γ} where $\gamma = 1, 2, 3, 4,$ and 5 is the identification number for each conductor as shown in Fig. 3.1. Conductivity of the core conductors and sheath is termed as σ^{γ} which varies along x and y coordinates. We assume that along z co-ordinate σ^{γ} is constant. Since we have 5 separate conductors so we have to write 5 different VIEs and create SLAEs as follows

$$j^{\gamma}(\boldsymbol{\rho})/\sigma^{\gamma} + i\omega\mu_0 \sum_{\zeta=1}^{5} \iint_{S^{\zeta}} ds' G_0(\boldsymbol{\rho}, \boldsymbol{\rho}') j^{\zeta}(\boldsymbol{\rho}') = V^{\gamma}_{\text{p.u.l.}}, \quad \boldsymbol{\rho} \in S^{\gamma}, \tag{3.1}$$

where $\gamma = 1, 2, 3, 4,$ and 5, $G_0(\boldsymbol{\rho}, \boldsymbol{\rho}') = -1/(2\pi)\ln(|\boldsymbol{\rho} - \boldsymbol{\rho}'|)$ is the free space Green's function, and $V^{\gamma}_{\text{p.u.l.}}$ is the per unit length voltage drop for the γ-th conductor along z coordinate. The unknowns of (3.1) are the volumetric polarization current densities j^{γ} flowing through each γ-th conductor.

Volumetric polarization current densities for each observation point $\boldsymbol{\rho}'$ inside the object can be calculated with superposition of fields contributed by all the point sources located at $\boldsymbol{\rho}''$ in the boundary as [25]. By using this theory polarization current j^{γ} can be expressed as

$$j^{\gamma}(\boldsymbol{\rho}') = -i\omega\mu_0 \oint_{\partial S^{\gamma}} d\boldsymbol{\rho}'' G_{\sigma^{\gamma}}(\boldsymbol{\rho}', \boldsymbol{\rho}'') J^{\gamma}(\boldsymbol{\rho}''), \quad \boldsymbol{\rho}' \in S^{\gamma}, \tag{3.2}$$

where J^{γ} is the unknown fictitious current in the boundary ∂S^{γ} and $G_{\sigma^{\gamma}}$ is the Green's function of the conducting media defined as

$$G_{\sigma^{\gamma}}(\boldsymbol{\rho}', \boldsymbol{\rho}'') = \frac{1}{4\,i} H_0^{(2)}(k_{\sigma^{\gamma}}|\boldsymbol{\rho}' - \boldsymbol{\rho}''|) \tag{3.3}$$

where σ^{γ} is the conductivity and $k_{\sigma^{\gamma}} = \sqrt{-i\omega\mu_0\sigma^{\gamma}}$ is the wavenumber of the same γ-th conductive media. Since $G_{\sigma^{\gamma}}$ satisfies the homogenous Helmholtz equation as

$$\nabla^2 G_{\sigma^{\gamma}}(\boldsymbol{\rho}', \boldsymbol{\rho}'') + k^2_{\sigma^{\gamma}} G_{\sigma^{\gamma}}(\boldsymbol{\rho}', \boldsymbol{\rho}'') = 0, \quad \boldsymbol{\rho}' \in S^{\gamma} - \partial S^{\gamma}, \quad \boldsymbol{\rho}'' \in \partial S^{\gamma}, \tag{3.4}$$

we can also say that j^{γ} (3.2) will also satisfy the same Helmholtz equation.

We can plug polarization current j^{γ} from (3.2) into (3.1) and write SVS-EFIE for 5 conductors as follows

$$\begin{bmatrix} \mathcal{T}_{\sigma^1}^{\partial S^1,\partial S^1} \circ J^1 \\ \vdots \\ \mathcal{T}_{\sigma^5}^{\partial S^5,\partial S^5} \circ J^5 \end{bmatrix} + \begin{bmatrix} \mathcal{T}_{0}^{\partial S^1,S^1} & \cdots & \mathcal{T}_{0}^{\partial S^1,S^5} \\ \vdots & \ddots & \vdots \\ \mathcal{T}_{0}^{\partial S^5,S^1} & \cdots & \mathcal{T}_{0}^{\partial S^5,S^5} \end{bmatrix} \circ \begin{bmatrix} \mathcal{T}_{\sigma^1}^{S^1,\partial S^1} \circ J^1 \\ \vdots \\ \mathcal{T}_{\sigma^5}^{S^5,\partial S^5} \circ J^5 \end{bmatrix} = \begin{bmatrix} \sigma^1 V_{\text{p.u.l.}}^1 \\ \vdots \\ \sigma^5 V_{\text{p.u.l.}}^5 \end{bmatrix} \tag{3.5}$$

The integral operators in (3.5) are defined as

$$\mathcal{T}_{\sigma^\gamma}^{\partial S^\gamma,\partial S^\gamma} \circ J^\gamma = -i\omega\mu_0 \oint_{\partial S^\gamma} d\boldsymbol{\rho}'' G_{\sigma^\gamma}(\boldsymbol{\rho},\boldsymbol{\rho}'') J^\gamma(\boldsymbol{\rho}''), \tag{3.6}$$

$$\mathcal{T}_{\sigma^\gamma}^{S^\gamma,\partial S^\gamma} \circ J^\gamma = -i\omega\mu_0 \oint_{\partial S^\gamma} d\boldsymbol{\rho}'' G_{\sigma^\gamma}(\boldsymbol{\rho}',\boldsymbol{\rho}'') J^\gamma(\boldsymbol{\rho}''), \tag{3.7}$$

$$\mathcal{T}_{0}^{\partial S^\gamma,S^\zeta} \circ j^\zeta = i\omega\mu_0\sigma^\gamma \iint_{S^\zeta} ds' G_0(\boldsymbol{\rho},\boldsymbol{\rho}') j^\zeta(\boldsymbol{\rho}'), \tag{3.8}$$

where $\gamma, \zeta = 1, 2, 3, 4,$ and 5.

3.3 HO-MoM Solution of the SVS-EFIE for a Sector Shaped MTLs

3.3.1 HO-MoM Geometrical Representation of a Sector Shaped MTL via Lagrange Interpolation

Although unknowns of SVS-EFIE (3.5) are in the boundary of the conductors we have to discretize both cross section and boundary of each γ-th conductor in order to represent the electric field in the cross-sections. Each boundary ∂S^γ is divided into M^γ HO curved line elements. Each cross section S^γ is divided into N^γ number of HO curved quadrilateral elements. This discretization results in total $M = M^1 + M^2 + M^3 + M^4 + M^5$ number of HO curvilinear line elements and $N = N^1 + N^2 + N^3 + N^4 + N^5$ number of HO curvilinear quadrilateral patches. Important point to notice here is sheath has two separate boundaries so M^5 counts elements on both of them.

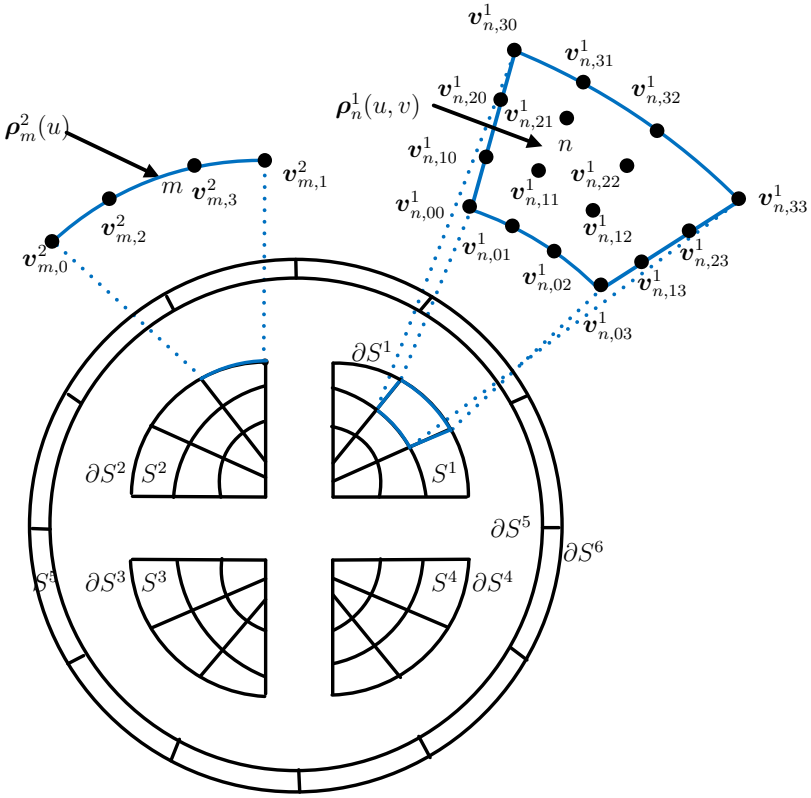

Figure 3.1: Mesh of a sector shaped MTLs showing third order HO line elements and quadrilateral elements.

In order to obtain HO 1-D and 2-D position-vectors on the boundary and cross section of the conductors we need to approximate them with HO Lagrangian type 1-D and 2-D type shape functions subsequently. The advantage of HO Lagrangian type interpolation is that it reduces the error in geometry very rapidly when we increase the order of Lagrange polynomials [60]. It is simple to program as well. Small number of Lagrangian type HO elements can be used to gain accurate geometry representation. Other types of interpolation schemes such as Non-Uniform Rational B-Spline (NURBS) [33] can also be used to represent object's geometry. One key advantage of NURBS based geometry is they can represent canonical objects like circles or ellipse exactly [68]. NURBS can also represent sophisticated objects of arbitrary shapes precisely by using small number of NURBS surfaces which is essential in reducing computational resources [66].

The 1-D shape function of geometrical order χ for representing the position vector on boundary can be expressed as [60]

$$L_\iota(u) = \prod_{p=0,\iota\neq p}^{\chi} \frac{u-u_p}{u_\iota-u_p}, \quad u \in [-1,1], \tag{3.9}$$

where $u_p = {}^{2p}/_{\chi} - 1$ and $\iota, p = 0, 1, \ldots, \chi$.

The position vector on m th 1D higher order line element on the boundary of γ-th conductor can be expressed with Lagrangian polynomial as [5, 59]

$$\boldsymbol{\rho}_m^\gamma(u) = \sum_{\iota=0}^{\chi} \boldsymbol{v}_{m,\iota}^\gamma \; L_\iota(u), \quad u \in [-1,1], \tag{3.10}$$

where $m = 0, 1, \ldots, M^\gamma - 1$, $\boldsymbol{v}_{m,\iota}^\gamma$ is the ι-th vertex of m-th Higher order line element of the boundary of γ-th conductor, and $\gamma = 1, 2, 3, 4,$ and 5.

Subsequently, Jacobian of m-th 1-D higher order curved line element part of the boundary of γ-th conductor can be defined as [5]

$$f_m^\gamma(u) = |\boldsymbol{a}^\gamma(u)|, \tag{3.11}$$

where unitary vector $\boldsymbol{a}^\gamma(u) = \frac{\partial}{\partial u}(\boldsymbol{\rho}_m^\gamma(u))$. By integrating the 1-D Jacobian (3.11) over a m-th HO line element with respect to parametric coordinate u, we can compute the length of that m-th HO line element.

Similarly, 2-D shape function of geometrical order χ for representing position vector on cross-section S^γ can be expressed as [59, 60]

$$L_{\iota\kappa}(u,v) = \prod_{p=0,\iota\neq p}^{\chi} \frac{u-u_p}{u_\iota-u_p} \prod_{q=0,\kappa\neq q}^{\chi} \frac{v-u_q}{u_\kappa-u_q}, \quad u,v \in [-1,1], \tag{3.12}$$

where $u_q = ({}^{2q}/_{\chi}) - 1$ and $\iota, \kappa = 0, 1, \ldots, \chi$. The 2-D position vector on n-th HO quadrilateral element on the volume of γ-th conductor can be expressed by using

Lagrangian polynomial as [5]

$$\boldsymbol{\rho}_n^{\gamma}(u,v) = \sum_{\iota=0}^{\chi}\sum_{\kappa=0}^{\chi} \boldsymbol{v}_{n,\iota\kappa}^{\gamma} L_{\iota\kappa}(u,v), \quad u,v \in [-1,1], \tag{3.13}$$

where $n = 0, 1, \ldots, N^{\gamma} - 1$, $\boldsymbol{v}_{n,\iota\kappa}^{\gamma}$ is the $\iota\kappa$-th vertex of n-th HO quadrilateral in the cross section of γ-th conductor, and $\gamma = 1, 2, 3, 4,$ and 5.

Subsequently, Jacobian of n-th 2-D higher order element part of the volume of γ-th conductor can be defined as [5]

$$f_n^{\gamma}(u,v) = \sqrt{|\bar{\bar{g}}_n^{\gamma}(u,v)|}, \tag{3.14}$$

where $\bar{\bar{g}}_n^{\gamma}(u,v)$ is a (2×2) matrix given as [5]

$$\bar{\bar{g}}_n^{\gamma}(u,v) = \begin{bmatrix} (\boldsymbol{a}_u^{\gamma} \cdot \boldsymbol{a}_u^{\gamma}) & (\boldsymbol{a}_u^{\gamma} \cdot \boldsymbol{a}_v^{\gamma}) \\ (\boldsymbol{a}_v^{\gamma} \cdot \boldsymbol{a}_u^{\gamma}) & (\boldsymbol{a}_v^{\gamma} \cdot \boldsymbol{a}_v^{\gamma}) \end{bmatrix},$$

the unitary vectors $\boldsymbol{a}_u^{\gamma}$ and $\boldsymbol{a}_v^{\gamma}$ are defined as [5]

$$\boldsymbol{a}_u^{\gamma} = \frac{\partial}{\partial u}(\boldsymbol{\rho}_n^{\gamma}(u,v)), \tag{3.15}$$

$$\boldsymbol{a}_v^{\gamma} = \frac{\partial}{\partial v}(\boldsymbol{\rho}_n^{\gamma}(u,v)). \tag{3.16}$$

By integrating the 2-D Jacobian (3.14) over a n-th HO quadrilateral element with respect to parametric coordinate u and v, we can compute the area of that n-th quadrilateral element.

3.3.2 HO Approximation of Fictitious Surface Currents and Volumetric Polarization Currents

To approximate unknown fictitious surface current J^{γ} on the boundary we have to use HO monomial basis function given as [67]

$$B_{\xi}(u) = u^{\xi}, \quad u \in [-1, 1], \tag{3.17}$$

where $\xi = 0, 1, \ldots, \Omega - 1$ and Ω is the highest order of monomial basis function. As we increase the order of monomial it will be able to capture the J^{γ} with more accuracy by introducing more unknowns.

Thus, the fictitious current J^{γ} on the boundary of the γ-th conductor can be approximated by using B_{ξ} (3.17) as [67]

$$J^{\gamma}(u) \cong \sum_{m=0}^{M^{\gamma}-1} \sum_{\xi=0}^{\Omega-1} I^{\gamma}_{m,\xi} B_{\xi}(u), \quad u \in [-1, 1], \tag{3.18}$$

where $\gamma = 1, 2, 3, 4,$ and 5, and $I^{\gamma}_{m,\xi}$ is the sought unknown coefficient of 1-D HO basis function B_{ξ} (3.17).

Similarly, to approximate unknown volumetric polarization current j^{γ} on the cross-section we have to use following HO basis function

$$b_{\xi'\psi'}(u, v) = u^{\xi'} v^{\psi'}, \quad u, v \in [-1, 1], \tag{3.19}$$

where $\xi', \psi' = 0, 1, \ldots, \Psi - 1$ and Ψ is the highest order of 2-D HO basis function $b_{\xi'\psi'}$ (3.19).

Thus, the volumetric polarization current j^{γ} in the cross-section S^{γ} of γ-th conductor can be approximated by using $b_{\xi'\psi'}$ (3.19) as [67]

$$j^{\gamma}(u, v) \cong \sum_{n=0}^{N^{\gamma}-1} \sum_{\xi'=0}^{\Psi-1} \sum_{\psi'=0}^{\Psi-1} i^{\gamma}_{n,\xi'\psi'} b_{\xi'\psi'}(u, v), \quad u, v \in [-1, 1], \tag{3.20}$$

where $\gamma = 1, 2, 3, 4,$ and 5.

3.3.3 Integral Representation of Surface-to-Volume Operator $\mathcal{T}_{\sigma}^{S,\partial S}$

Operator $\mathcal{T}_{\sigma}^{S,\partial S}$ (3.7) translates the field from the boundary of the γ-th conductor to the cross section of the same conductor and contributes to the polarization current by using Green's function of the conductive media G_{σ^γ} (3.3). According to HO-MoM [67], operator $\mathcal{T}_{\sigma}^{S,\partial S}$ can be represented in integral form by discretizing it with 1-D basis function $B_{\xi''}$ (3.17) and then testing with 2-D basis function $b_{\xi'\psi'}$ (3.19) as follows

$$\begin{aligned}\mathcal{Z}_{\xi'\psi',\xi''}^{S_{n'}^{\gamma},\partial S_{m''}^{\gamma}} &= \langle b_{\xi'\psi'}, \langle G_{\sigma^\gamma}, B_{\xi''}\rangle\rangle \\ &= -i\omega\mu_0 \int_{-1}^{1}\int_{-1}^{1} du'dv' b_{\xi'\psi'}(u',v') f_{n'}^{\gamma}(u',v') \\ &\times \int_{-1}^{1} du'' B_{\xi''}(u'') G_{\sigma^\gamma}(\boldsymbol{\rho}_{n'}^{\gamma}(u',v'), \boldsymbol{\rho}_{m''}^{\gamma}(u'')) f_{m''}^{\gamma}(u''),\end{aligned} \tag{3.21}$$

where $f_{n'}^{\gamma}(u',v')$ (3.14) is the Jacobian of n'-th 2-D higher order element which belongs to the cross-section S^γ and $f_{m''}^{\gamma}(u'')$ (3.11) is the Jacobian of the m''-th 1-D higher order curved line element which belongs to the boundary ∂S^γ.

After computing each interaction $\mathcal{Z}_{\xi'\psi',\xi''}^{S_{n'}^{\gamma},\partial S_{m''}^{\gamma}}$ between m''-th contour element for 1-D basis function of order ξ'' and n'-th cross sectional quadrilateral element for 2-D basis function of order $\xi'\psi'$ we have to assemble them in a matrix $Z_{\sigma^\gamma}^{S^\gamma,\partial S^\gamma}$ as follows

$$\left[Z_{\sigma^\gamma}^{S^\gamma,\partial S^\gamma}\right]_{p',q''} = \mathcal{Z}_{\xi'\psi',\xi''}^{S_{n'}^{\gamma},\partial S_{m''}^{\gamma}}, \tag{3.22}$$

where $p' = n'\Psi^2 + \xi'\Psi + \psi'$ and $q'' = m''\Omega + \xi''$ are the row and column index of the matrix $Z_{\sigma^\gamma}^{S^\gamma,\partial S^\gamma}$, $n' = 0, 1, \ldots, N^\gamma - 1$ is the id number of quadrilateral which belongs to cross-section S^γ, $\xi', \psi' = 0, 1, \ldots, \Psi - 1$ are the orders of 2-D HO basis (3.19), the index of line element which belongs to the boundary ∂S^γ is termed as $m'' = 0, 1, \ldots, M^\gamma - 1$, and $\xi'' = 0, 1, \ldots, \Omega - 1$ is the order of 1-D HO basis (3.17).

3.3.4 Integral Representation of Volume-to-Surface Operator $\mathcal{T}_0^{\partial S,S}$

Operator $\mathcal{T}_0^{\partial S,S}$ (3.8) translates the polarization current j^ζ from the volume of ζ-th conductor to the boundary of γ-th conductor and contributes to the tangential component of electric field by using Green's function of the free space G_0 (2.14). According to HO-MoM [67], operator $\mathcal{T}_0^{\partial S,S}$ can be represented in integral form by discretizing it with 2-D basis function $b_{\xi'\psi'}$ (3.19) and then testing with 1-D test function B_ξ (3.17) as following

$$\begin{aligned}\mathcal{Z}_{\xi,\xi'\psi'}^{\partial S_m^\gamma, S_{n'}^\zeta} &= \langle B_\xi, \langle G_0, b_{\xi'\psi'}\rangle\rangle \\ &= i\omega\mu_0\sigma^\gamma \int_{-1}^{1} du B_\xi(u) f_m^\gamma(u) \int_{-1}^{1}\int_{-1}^{1} du'dv' b_{\xi'\psi'}(u',v') \\ &\qquad \times f_{n'}^\zeta(u',v') G_0(\boldsymbol{\rho}_m^\gamma(u), \boldsymbol{\rho}_{n'}^\zeta(u',v')),\end{aligned} \tag{3.23}$$

where $f_{n'}^\zeta(u',v')$ is same as (3.14) except the fact that we need to use ζ instead of γ, is the Jacobian of n'-th 2-D higher order quad element which belongs to cross-section S^ζ and $f_m^\gamma(u)$ (3.11) is the Jacobian of the m-th 1-D higher order curved line element which belongs to the boundary ∂S^γ.

After computing each interaction $\mathcal{Z}_{\xi,\xi'\psi'}^{\partial S_m^\gamma, S_{n'}^\zeta}$ between n'-th cross sectional quadrilateral element for 2-D basis function of order $\xi'\psi'$ and m-th contour element for 1-D basis function of order ξ we have to assemble them in a matrix as

$$\left[Z_0^{\partial S^\gamma, S^\zeta}\right]_{q,p'} = \mathcal{Z}_{\xi,\xi'\psi'}^{\partial S_m^\gamma, S_{n'}^\zeta}, \tag{3.24}$$

where $q = m\Omega + \xi$ and $p' = n'\Psi^2 + \xi'\Psi + \psi'$ are the row and column index of the matrix $Z_0^{\partial S^\gamma, S^\zeta}$, $\xi', \psi' = 0, 1, \ldots, \Psi - 1$ are the orders of 2-D basis function (3.19), $n' = 0, 1, \ldots, N^\zeta - 1$ is theid number of the quadrilateral element which belongs to cross-section S^ζ, the ID's of line element which belongs to the boundary ∂S^γ is termed as $m = 0, 1, \ldots, M^\gamma - 1$, and $\xi = 0, 1, \ldots, \Omega - 1$ is the order of 1-D HO basis function (3.17).

3.3.5 Integral Representation of Surface-to-Surface Operator $\mathcal{T}_{\sigma}^{\partial S,\partial S}$

Operator $\mathcal{T}_{\sigma}^{\partial S,\partial S}$ (3.6) translates the field from the boundary of the γ-th conductor to the boundary of the same conductor and contributes to the total electric field by using Green's function of the conductive media G_{σ^γ} (3.3). According to HO-MoM [67],, operator $\mathcal{T}_{\sigma}^{\partial S,\partial S}$ can be represented in integral form by discretizing it with 1-D basis function $B_{\xi''}$ (3.17) and then testing with 1-D test function B_{ξ} (3.17) as follows

$$\begin{aligned}\mathcal{Z}_{\xi,\xi''}^{\partial S_m^\gamma,\partial S_{m''}^\gamma} &= \langle B_\xi, \langle G_{\sigma^\gamma}, B_{\xi''}\rangle\rangle \\ &= -i\omega\mu_0 \int_{-1}^{1} du B_\xi(u) f_m^\gamma(u) \\ &\quad \times \int_{-1}^{1} du'' B_{\xi''}(u'') f_{m''}^\gamma(u'') G_{\sigma^\gamma}(\boldsymbol{\rho}_m^\gamma(u), \boldsymbol{\rho}_{m''}^\gamma(u'')),\end{aligned} \tag{3.25}$$

where $f_m^\gamma(u)$ (3.11) is the Jacobian of the m-th 1-D higher order curved line element and $f_{m''}^\gamma(u'')$ (3.11) is the Jacobian of the m''-th 1-D higher order curved line element which belongs to the boundary ∂S^γ.

After computing each interaction $\mathcal{Z}_{\xi,\xi''}^{\partial S_m^\gamma,\partial S_{m''}^\gamma}$ between m''-th contour element for 1-D HO basis function of order ξ'' and m-th contour element for 1-D test function of order ξ we have to assemble them in a matrix $Z_{\sigma^\gamma}^{\partial S^\gamma,\partial S^\gamma}$ as following

$$\left[Z_{\sigma^\gamma}^{\partial S^\gamma,\partial S^\gamma}\right]_{q,q''} = \mathcal{Z}_{\xi,\xi''}^{\partial S_m^\gamma,\partial S_{m''}^\gamma}, \tag{3.26}$$

where $q = m\Omega + \xi$, $q'' = m''\Omega + \xi''$ are the row and column indexes of the matrix $Z_{\sigma^\gamma}^{\partial S^\gamma,\partial S^\gamma}$, the index of line elements, which belongs to the boundary ∂S^γ is termed as $m, m'' = 0, 1, \ldots, M^\gamma - 1$, and $\xi, \xi'' = 0, 1, \ldots, \Omega - 1$ are the powers of 1-D HO basis function (3.17).

3.3.6 Integral Representation of $V_{p.u.l.}$

The right hand side for creating SLAE (3.29) can be computed by testing the discretized form of per unit length voltage drop $V^{\gamma}_{\text{p.u.l.}}$ in the γ-th conductor with 1-D HO test function B_{ξ} (3.17) as follows

$$\mathcal{V}^{\gamma}_{m,\xi} = \langle B_{\xi}, V^{\gamma}_{\text{p.u.l.}} \rangle = V^{\gamma}_{\text{p.u.l.}} \sigma^{\gamma} \int_{-1}^{1} du B_{\xi}(u) f^{\gamma}_{m}(u). \tag{3.27}$$

Each interaction is then stored in a vector as follows

$$[V^{\gamma}]_{q} = \mathcal{V}^{\gamma}_{m,\xi}, \tag{3.28}$$

where $q = m\Omega + \xi$, $f^{\gamma}_{m}(u)$ (3.11) is the Jacobian of the m-th 1-D curved HO element, the indexes of each line element belongs to ∂S^{γ} is termed as $m = 0, 1, \ldots, M^{\gamma} - 1$, and $\xi = 0, 1, \ldots, \Omega - 1$ is the order of 1-DHO test function (3.17).

3.3.7 Solving SLAE Created by HO-MoM Solution of SVS-EFIE (3.5)

For 5 conductors of a sectorial cable, how the local surface-to-volume matrix $\left[Z^{S^{\gamma},\partial S^{\gamma}}_{\sigma^{\gamma}}\right]$ (3.22), volume-to-surafce matrix $\left[Z^{\partial S^{\gamma},S^{\zeta}}_{0}\right]$ (3.24), surface-to-surface matrix $\left[Z^{\partial S^{\gamma},\partial S^{\gamma}}_{\sigma^{\gamma}}\right]$ (3.26), and right hand side local vector $[V^{\gamma}]$ (3.28) for γ-th conductor are assembled into the final global matrices $\left[Z^{S,\partial S}_{\sigma}\right]$, $\left[Z^{\partial S,S}_{0}\right]$, $\left[Z^{\partial S,\partial S}_{\sigma}\right]$, and global right hand side vector $[V]$ respectively is shown in (3.29).

Integral operators $\mathcal{T}^{S,\partial S}_{\sigma}$, $\mathcal{T}^{\partial S,S}_{0}$, $\mathcal{T}^{\partial S,\partial S}_{\sigma}$ are discretized and tested with appropriate basis functions and p.u.l. voltage drop $V_{\text{p.u.l.}}$is tested with appropriate basis functions to fill all the global matrices and right side vector. Finally all these global matrices and right side vector along with the global Gram matrix [62] form a System of Linear Algebraic Equation (SLAE) with respect to the unknown coefficients $[I]$ as follows

$$\Big(\underbrace{\left[Z^{\partial S,\partial S}_{\sigma}\right]}_{M\Omega\times M\Omega} + \underbrace{\left[Z^{\partial S,S}_{0}\right]}_{M\Omega\times N\Psi^2} \cdot \underbrace{[\Gamma]^{-1}}_{N\Psi^2\times N\Psi^2} \cdot \underbrace{\left[Z^{S,\partial S}_{\sigma}\right]}_{N\Psi^2\times M\Omega} \Big) \cdot \underbrace{[I]}_{M\Omega\times 1} = \underbrace{[V]}_{M\Omega\times 1}, \tag{3.30}$$

$$
\begin{bmatrix} \underbrace{[V^1]}_{M^1\Omega\times 1} \\ \vdots \\ \underbrace{[V^5]}_{M^5\Omega\times 1} \end{bmatrix} = \Bigg(\begin{bmatrix} \underbrace{\left[Z_{\sigma^1}^{\partial S^1,\partial S^1}\right]}_{M^1\Omega\times M^1\Omega} & & 0 \\ & \ddots & \\ 0 & & \underbrace{\left[Z_{\sigma^5}^{\partial S^5,\partial S^5}\right]}_{M^5\Omega\times M^5\Omega} \end{bmatrix} + \begin{bmatrix} \underbrace{\left[Z_0^{\partial S^1,S^1}\right]}_{M^1\Omega\times N^1\Psi^2} & \cdots & \underbrace{\left[Z_0^{\partial S^1,S^5}\right]}_{M^1\Omega\times N^5\Psi^2} \\ \vdots & \ddots & \vdots \\ \underbrace{\left[Z_0^{\partial S^5,S^1}\right]}_{M^5\Omega\times N^1\Psi^2} & \cdots & \underbrace{\left[Z_0^{\partial S^5,S^5}\right]}_{M^5\Omega\times N^5\Psi^2} \end{bmatrix} \cdot \begin{bmatrix} \underbrace{\left[\Gamma^{S^1,S^1}\right]}_{N^1\Psi^2\times N^1\Psi^2} & & 0 \\ & \ddots & \\ 0 & & \underbrace{\left[\Gamma^{S^5,S^5}\right]}_{N^5\Psi^2\times N^5\Psi^2} \end{bmatrix}^{-1} \cdot \begin{bmatrix} \underbrace{\left[Z_{\sigma^1}^{S^1,\partial S^1}\right]}_{N^1\Psi^2\times M^1\Omega} & & 0 \\ & \ddots & \\ 0 & & \underbrace{\left[Z_{\sigma^5}^{S^5,\partial S^5}\right]}_{N^5\Psi^2\times M^5\Omega} \end{bmatrix} \Bigg) \cdot \begin{bmatrix} \underbrace{[I^1]}_{M^1\Omega\times 1} \\ \vdots \\ \underbrace{[I^5]}_{M^5\Omega\times 1} \end{bmatrix} . \tag{3.29}
$$

where $[\Gamma]$ is the global block-diagonal Gram matrix [62] which is inner product between 2-D HO basis functions (3.19). Only the diagonal components of Gram matrix are non zero for our choice of basis functions. The Gram matrix represents the basis functions discretizing the domain of the volume-to-surface operator in terms of the test functions discretizing the surface-to-volume operator (3.17). Gram matrix elements are defined as the following inner products

$$
\Gamma_{p,p'}^{S^\gamma,S^\gamma}(\xi,\xi',\psi,\psi') = \int_{-1}^{1}\int_{-1}^{1} dudv f_n^\gamma(u,v) u^\xi v^\psi u^{\xi'} v^{\psi'}, \tag{3.31}
$$

where $p = n\Psi^2+\xi\Psi+\psi$, $p' = n'\Psi^2+\xi'\Psi+\psi'$ are the row and column indexes of Gram matrix, $f_n^\gamma(u,v)$ is the 2-D Jacobian (3.14), the indexes of 2-D HO quadrilaterals which belong to cross-section S^γ are termed as $n, n' = 0, 1, \ldots, N^\gamma - 1$, and $\xi, \xi', \psi, \psi' =$

$0, 1, \ldots, \Psi - 1$ are the orders of 2-D HO test function (3.19).

If we solve SLAEs (3.29) we can calculate the unknown coefficients $[I^{\gamma}]$ which can be used to find the unknown coefficient $[i^{\gamma}]$ of the volumetric polarization current densities (3.20) as

$$[i^{\gamma}] = i\omega\mu_0 \left[\Gamma^{S^{\gamma},S^{\gamma}}\right]^{-1} \cdot \left[Z_{\sigma^{\gamma}}^{S^{\gamma},\partial S^{\gamma}}\right] \cdot [I^{\gamma}]\,. \tag{3.32}$$

Once we compute polarization current densities we can compute the admittance matrix by integrating them throughout the cross-section and the invert the admittance matrix to obtain impedance matrix. We place the sector shaped cable into the center of a cylindrical cavity. Hence, for 6 conductors we can write (5×5) p.u.l. impedance matrix (cylindrical cavity is considered as reference conductor) as following

$$\bar{\bar{Z}} = \begin{bmatrix} Z_1 & Z_2 & Z_3 & Z_2 & Z_4 \\ Z_2 & Z_1 & Z_2 & Z_3 & Z_4 \\ Z_3 & Z_2 & Z_1 & Z_2 & Z_4 \\ Z_2 & Z_3 & Z_2 & Z_1 & Z_4 \\ Z_4 & Z_4 & Z_4 & Z_4 & Z_5 \end{bmatrix}$$

Since sectorial cable is a symmetrical MTLs so we can fill up the whole (5×5) matrix by using only Z_1, Z_2, Z_3, Z_4, and Z_5 [2].

3.4 Numerical Results

To demonstrate SVS-EFIE's capability to extract accurate p.u.l. resistance and inductance for sophisticated MTL, we use the example of a sector shaped cable which consists of 4 core sector shaped conductors and one sheath around them as shown in Fig. 3.2. First, we discretize the contour of all conductors of a sectorial cable with second order line elements and cross-sections with second order quadrilateral elements, which are created based on Lagrangian interpolators for the HO element radius-vectors. After that SVS-EFIE is solved with HO-MoM to calculate the volumetric polarization current. HO-FEM from the commercial COMSOL [51] software is also used to obtain the reference solution for the same volumetric polarization cur-

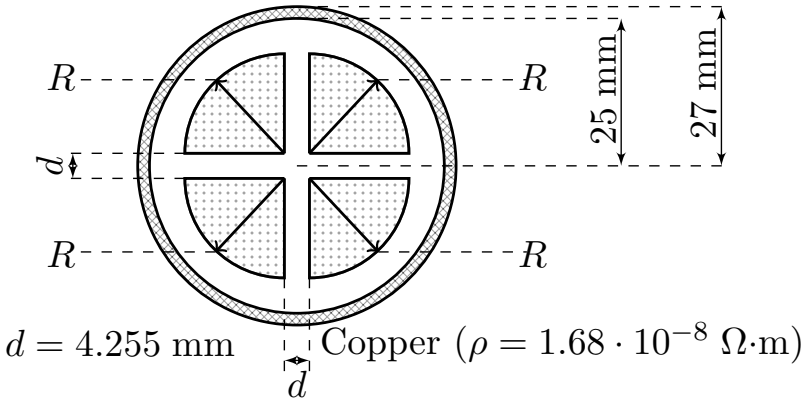

Figure 3.2: Geometry of sectorial cable with 4 sectors each having radius $R = 19mm - \frac{d}{2}$ and one sheath around them for p.u.l. resistance and inductance extraction.

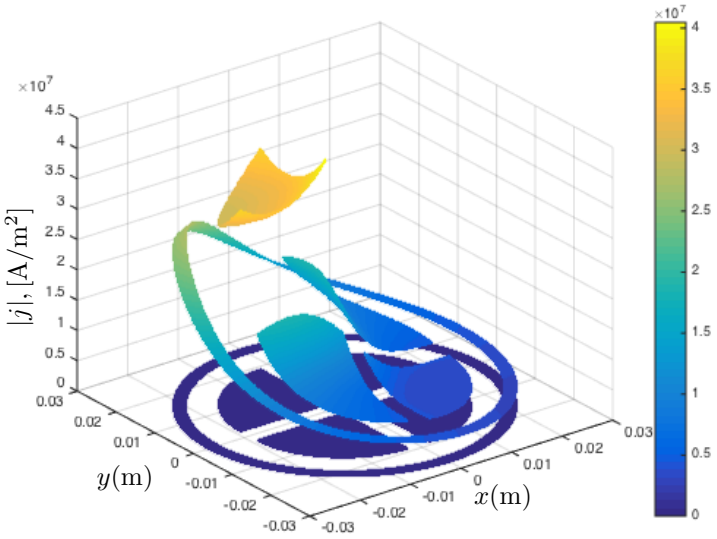

Figure 3.3: Magnitude of volumetric current densities j at 60 Hz in 4-sector cable obtained via 3rd order HO MoM solution of SVS-EFIE for $M = 360$ second order contour and $N = 500$ volume elements.

rents. Detailed descriptions of HO-COMSOL can be found in the appendix section of this thesis.

To obtain volumetric current densities for sectorial cable shown in Fig. 3.2 we solve SVS-EFIE with 3rd order solution of HO-MoM by discretizing the boundaries with 360 second order line elements and 500 second order quadrilaterals. Volumetric polarization current densities are obtained by using SVS-EFIE when 1st core is excited

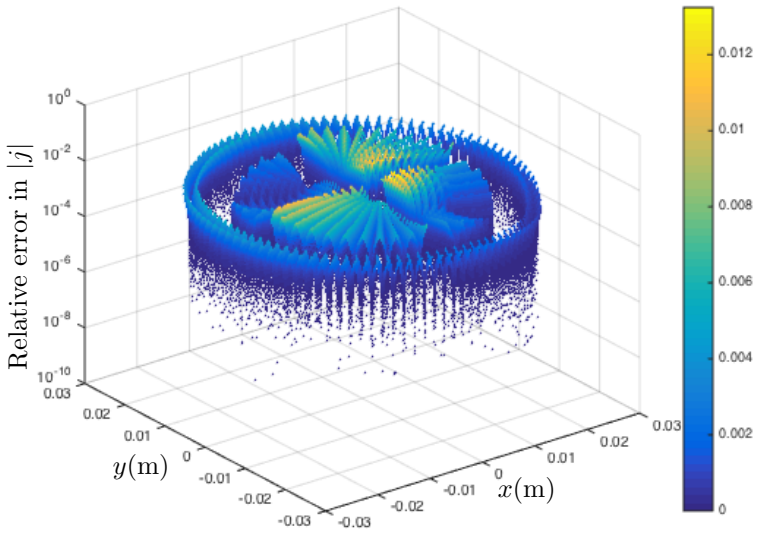

Figure 3.4: Relative error in amplitude of polarization current densities j for 4-sector cable between 3rd order HO MoM solution of SVS-EFIE and 3rd order COMSOL [51] at 60 Hz for $M = 360$ contour and $N = 500$ volume elements.

with 1 $^{V}/_{m}$ and rest of the three sectors and the sheath are grounded. Fig. 3.3 shows volumetric current distribution at 60 Hz. Proximity effect is clearly visible in Fig. 3.3. Then we simulate the same sectorial cable by using 3rd order COMSOL where its boundaries are discretized with 500 line elements and the whole domain contains 29, 706 triangular elements. Fig. 3.4 shows the relative error in volumetric current distribution between HO-MoM based SVS-EFIE (3.29) and COMSOL [51]. Memory requirement for HO-MoM based SVS-EFIE substantially smaller than HO-FEM based COMSOL [51] because the number of unknowns for SVS-EFIE is much smaller than FEM [59]. Since sector shaped cable is symmetrical so we fill the whole (5×5) impedance matrix with only Z_1, Z_2, Z_3, Z_4, and Z_5 as [2].

Table 3.1 shows all 5 impedance values needed to compute the whole impedance matrix at frequencies 60 Hz and 1000 Hz. One can clearly see at 60 Hz impedance values obtained by SVS-EFIE have 5 digit agreement with HO-COMSOL.

Fig. 3.5 and Fig. 3.6 show the convergence in relative error in the p.u.l. resistive and inductive part respectively for one of the five impedance values, $Z_1^{\text{svs}} = R_1 + j\omega L_1$ between HO-MoM solution of SVS-EFIE and HO-COMSOL at 60 Hz for a sectorial

Table 3.1: P.u.l. impedance Z in $[m\Omega/m]$ computed using 3rd order HO-MoM solution ($\Omega = \Phi = 3$) of SVS-EFIE (3.5) with $M = 360$ contour and and $N = 500$ volume elements for Sector shaped cable. Order 3 FEM solutions with $29,706$ elements [51] are provided for reference.

60 Hz			1000 Hz		
	R	$j\omega L$		R	$j\omega L$
Z_1^{FEM}	0.09215553	0.3646721	Z_1^{FEM}	0.2696	5.514
Z_1^{SVS}	0.09215529	0.3646714	Z_1^{SVS}	0.2699	5.517
Z_2^{FEM}	0.00217439	0.2990032	Z_2^{FEM}	0.0409	4.893
Z_2^{SVS}	0.00217451	0.2990030	Z_2^{SVS}	0.0413	4.891
Z_3^{FEM}	-0.00722474	0.28142495	Z_3^{FEM}	0.00769	4.771
Z_3^{SVS}	-0.00722463	0.28142482	Z_3^{SVS}	0.00813	4.769
Z_4^{FEM}	$2.674 \cdot 10^{-5}$	0.27515892	Z_4^{FEM}	0.00679	4.5869
Z_4^{SVS}	$2.669 \cdot 10^{-5}$	0.27515889	Z_4^{SVS}	0.00716	4.5846
Z_5^{FEM}	0.05143318	0.27419270	Z_5^{FEM}	0.0548	4.572
Z_5^{SVS}	0.05143304	0.27419263	Z_5^{SVS}	0.0551	4.569

cable by varying order of HO-MoM solution and total number of quadrilateral element. For obtaining these two convergence curves Fig. 3.5 and Fig. 3.6, order of geometry was kept constant at 3rd order. HO-FEM based COMSOL [51] truncates its mesh at a certain distance away from the object and applies boundary condition. Because of this boundary condition field becomes zero at that boundary. To match the result obtained by HO-MoM based SVS-EFIE we need to apply same boundary condition. We apply the boundary condition by using Green's function of cylindrical cavity G_{cav} [59] instead of free space Green's function $G_0(\boldsymbol{\rho}, \boldsymbol{\rho}') = -1/(2\pi)\ln(|\boldsymbol{\rho} - \boldsymbol{\rho}'|)$.

3.5 Conclusions

This Chapter presents HO-MoM solution of SVS-EFIE to compute p.u.l. resistance and inductance matrices for sector shaped MTLs. Volumetric current distribution at 60 Hz has been shown in Fig. 3.3 and proximity effect is clearly visible. The

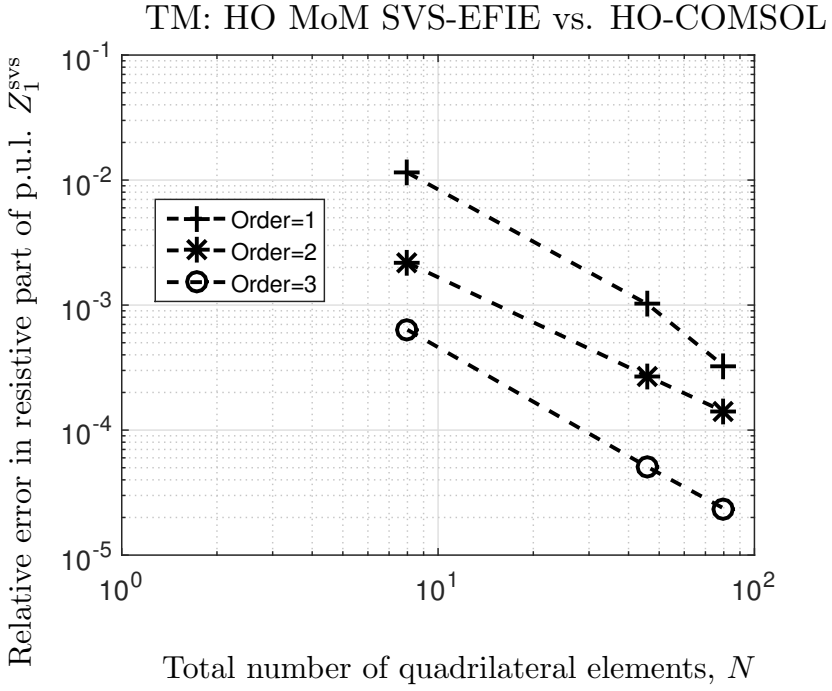

Figure 3.5: Relative error in the resistive part of impedance $Z_1^{\text{svs}} = R_1 + j\omega L_1$ in [mΩ/m] for sectorial cable depicted in Fig. 3.2 at 60 Hz between HO-MoM solution of SVS EFIE and HO-COMSOL by varying the order of solution along with total quadrilateral elements while the order of geometry was kept constant at order, $\chi = 3$ and total number of boundary element, $M = 4\sqrt{N}$.

aggressor conductor is set to 1 V/m p.u.l. voltage and rest of the victim conductors are set to 0V/m. The victim conductors return the same amount of current in opposite direction to that of the aggressor conductor. To demonstrate the accuracy in the volumetric current distribution, HO-MoM solution of SVS-EFIE was compared with HO-FEM of the COMSOL commercial software. The relative error is shown in Fig. 3.4. Table 3.1 shows the the comparison of p.u.l. impedance matrix values obtained by SVS-EFIE and HO-FEM of the COMSOL. One can see that HO-MoM solution of the SVS-EFIE agrees with HO-FEM solution of COMSOL up to 5 digits in p.u.l. resistance and inductance at 60 Hz but. When we increase the frequency the agreement drops to 2-3 digits at 1KHz because of the stronger skin effect. At this frequency current is varying more rapidly in regions near the boundary. In order to make HO-MoM solution of SVS-EFIE more accurate further mesh refinement,

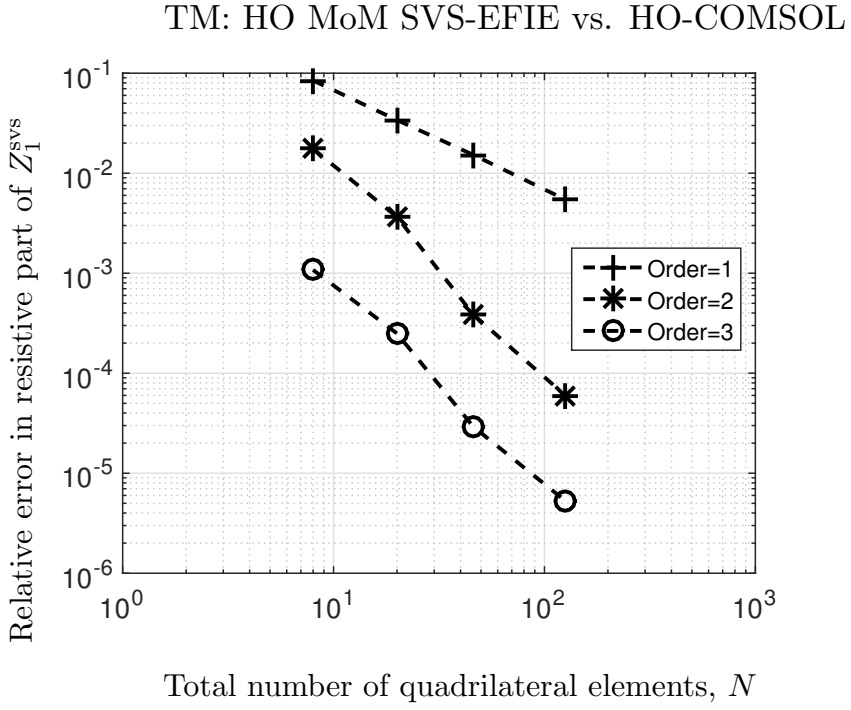

Figure 3.6: Relative error in the inductive part of p.u.l. impedance $Z_1^{\text{svs}} = R_1 + j\omega L_1$ in [μH/m] for sectorial cable depicted in Fig. 3.2 at 60 Hz between HO-MoM solution of SVS EFIE and HO-COMSOL by varying the order of solution along with total quadrilateral elements while the order of geometry was kept constant at order, $\chi = 3$ and total number of boundary element, $M = 4\sqrt{N}$.

increase in the solution order, and increase of the adaptive integration accuracy are required.

4

Higher Order Method of Moments Solution of the SVS-EFIE for Scalar TM Scattering by Homogeneous Non-Magnetic 2-D Cylinder

4.1 Scalar SVS-EFIE for 2-D TM Scattering

In Chapter 3, scalar SVS-EFIE (3.5) was formulated for quasi magneto-static analysis of current flow in MTLs under quasi-TM fields approximation. Similarly, scalar SVS-EFIE can be derived from VIE for full wave scattering on homogeneous dielectric objects under TM-polarization. If we consider a dielectric object with cross sectional area S we can write VIE for TM case as [14, 53]

$$E_z(\boldsymbol{\rho}) - k_0^2(\epsilon - 1)\iint_S G_0(\boldsymbol{\rho}, \boldsymbol{\rho}')E_z(\boldsymbol{\rho}')\, ds' = E_z^{\text{inc}}(\boldsymbol{\rho}), \boldsymbol{\rho} \in S, \tag{4.1}$$

where $E_z(\boldsymbol{\rho}')$ is the unknown distribution of the electric field inside the cylinder, $G_0(\boldsymbol{\rho}, \boldsymbol{\rho}') = -\frac{i}{4}H_0^{(2)}(k_0|\boldsymbol{\rho} - \boldsymbol{\rho}'|)$ is the Green's function of free space, i is the imagi-

nary unit, $H_0^{(2)}$ is the Hankel function of second kind and order zero, $k_0 = \omega\sqrt{\epsilon_0\mu_0}$ is the vacuum wavenumber, ϵ_0 is the permittivity of free space and μ_0 is the magnetic permeability of free space, ω is the angular frequency, the complex relative permittivity of the dielectric object is defined as $\epsilon = \varepsilon - i\sigma/(\omega\varepsilon_0)$, σ is the dielectric conductivity, and E_z^{inc} is the incident field.

Electric field E_z for each observation point $\boldsymbol{\rho}'$ inside the object can be calculated with superposition of fields contributed by all the point sources in the boundary ∂S as [25]

$$E_z(\boldsymbol{\rho}') = -i\omega\mu_0 \int_{\partial S} G_\epsilon(\boldsymbol{\rho}', \boldsymbol{\rho}'')\, \mathtt{J}_z(\boldsymbol{\rho}'')\, d\boldsymbol{\rho}'',\ \boldsymbol{\rho}' \in S. \tag{4.2}$$

In (4.2), $G_\epsilon(\boldsymbol{\rho}', \boldsymbol{\rho}'') = -\frac{i}{4}H_0^{(2)}(k_\epsilon|\boldsymbol{\rho}' - \boldsymbol{\rho}''|)$ is the Green's function of the dielectric object having wavenumber $k_\epsilon = \omega\sqrt{\mu_0\varepsilon_0\epsilon}$.

We know that for source points on the boundary $\boldsymbol{\rho}'' \in \partial S$ the Green's function of the dielectric object G_ϵ satisfies the Helmholtz equation with right hand side zero for all the observation points inside the object excluding boundary as

$$\nabla^2 G_\epsilon(\boldsymbol{\rho}', \boldsymbol{\rho}'') + k_\epsilon^2 G_\epsilon(\boldsymbol{\rho}', \boldsymbol{\rho}'') = 0, \quad \boldsymbol{\rho}' \in S. \tag{4.3}$$

Since G_ϵ satisfies Helmholtz equation, superposition of G_ϵ with some weighting function $\mathtt{J}_z$ will also satisfy the same equation. That means E_z, constructed as superposition of waves G_ϵ (2.21), satisfies the same homogeneous Helmholtz equation as

$$\nabla^2 E_z(\boldsymbol{\rho}') + k_\epsilon^2 E_z(\boldsymbol{\rho}') = 0, \quad \boldsymbol{\rho}' \in S. \tag{4.4}$$

The substitution of (4.2) into (4.1) gives us SVS-EFIE for TM scattering problem

as

$$-i\omega\mu_0 \int_{\partial S} G_\epsilon(\boldsymbol{\rho},\boldsymbol{\rho}'')\mathtt{J}_z(\boldsymbol{\rho}'')\,d\boldsymbol{\rho}'' + i\omega\mu_0 k_0^2(\epsilon-1)\iint_S G_0(\boldsymbol{\rho},\boldsymbol{\rho}')\times \int_{\partial S} G_\epsilon(\boldsymbol{\rho}',\boldsymbol{\rho}'')\mathtt{J}_z\,(\boldsymbol{\rho}'')\,d\boldsymbol{\rho}''ds' = E_z^{\text{inc}}(\boldsymbol{\rho}), \quad (4.5)$$

where observation points are located on the boundary of the scatterer $\boldsymbol{\rho} \in \partial S$. SVS-EFIE (4.5) can also be represented by using scalar operator $\mathtt{T}$ as following

$$\mathtt{T}_\epsilon^{\partial S,\partial S} \circ \mathtt{J}_z + \mathtt{T}_0^{\partial S,S} \circ \mathtt{T}_\epsilon^{S,\partial S} \circ \mathtt{J}_z = E^{\text{inc}}, \quad (4.6)$$

where the integral operators are defined as

$$\mathtt{T}_\epsilon^{\partial S,\partial S} \circ \mathtt{J}_z = -i\omega\mu_0 \int_{\partial S} G_\epsilon(\boldsymbol{\rho},\boldsymbol{\rho}'')\mathtt{J}_z(\boldsymbol{\rho}'')\,d\boldsymbol{\rho}'',\ \boldsymbol{\rho} \in \partial S, \quad (4.7)$$

$$\mathtt{T}_\epsilon^{S,\partial S} \circ \mathtt{J}_z = i\omega\mu_0 \int_{\partial S} G_\epsilon(\boldsymbol{\rho}',\boldsymbol{\rho}'')\mathtt{J}_z(\boldsymbol{\rho}'')\,d\boldsymbol{\rho}'',\ \boldsymbol{\rho}' \in S, \quad (4.8)$$

$$\mathtt{T}_0^{\partial S,S} \circ E_z = k_0^2(\epsilon-1)\iint_S G_0(\boldsymbol{\rho},\boldsymbol{\rho}')E_z(\boldsymbol{\rho}')\,ds',\ \boldsymbol{\rho} \in \partial S. \quad (4.9)$$

4.2 Higher Order Representation of Arbitrary Geometry

Higher Order representation of arbitrary geometry for sectorial cable was shown in Chapter 3. In this Chapter we will show the same formulation for a single circular dielectric cylinder. 1-D shape functions to define 1-D position vector can be expressed as [60]

$$S_i(u) = \prod_{n=0, i\neq n}^{\chi} \frac{u-u_n}{u_i-u_n}, \quad -1 \leqslant u \leqslant 1, \quad (4.10)$$

where $u_n = \frac{2n-\chi}{\chi}$, $n = 0, 1, ..., \chi$ and χ is the order of geometry for 1-D higher order curved line element. The position-vector on the m-th higher order curved line

element of the boundary of any arbitrary shaped scatterer shown in Fig. 4.1 is defined as [5]

$$\boldsymbol{\rho}_m(u) = \sum_{i=0}^{\chi} \boldsymbol{v}_{m,i}\ S_i(u), \quad -1 \leqslant u \leqslant 1, \tag{4.11}$$

where $m = 0, 1..., M-1$ and $\boldsymbol{v}_{m,i}$ is the i-th vertex of m-th HO line element.

Similarly, 2-D shape functions to define 2-D position vector can be expressed as [60]

$$S_{ij}(u,v) = \prod_{n=0, i\neq n}^{\chi} \frac{u-u_n}{u_i-u_n} \prod_{m=0, j\neq m}^{\chi} \frac{v-v_m}{v_j-v_m}, \tag{4.12}$$

where $-1 \leqslant u, v \leqslant 1$.

where $v_m = \frac{2m-\chi}{\chi}$, $n, m = 0, 1, ..., \chi$, and χ is the order of geometry for 2-D curved quad element in the cross-section.

The 2-D position-vector on the n-th HO 2-D quad element of any arbitrary shaped scatterer shown in Fig. 4.1 is defined as [5]

$$\boldsymbol{\rho}_n(u,v) = \sum_{i=0}^{\chi} \sum_{j=0}^{\chi} \boldsymbol{v}_{n,ij}\ S_{ij}(u,v), \tag{4.13}$$

where $-1 \leqslant u, v \leqslant 1$ and $n = 0, 1, ..., N-1$, N being the total number of quadrilateral patches. In (4.13), $\boldsymbol{v}_{n,ij}$ is the ij-th vertex of the n-th 2-D HO quad element in the cross-section of the object.

4.3 Higher Order MoM Solution of Scalar SVS-EFIE for Scattering by 2-D Dielectric Object

4.3.1 Surface and Volume Current Expansions

Unknown Surface current density $\mathtt{J}_z(\boldsymbol{\rho}_m(u))$ in (4.6) can be discretized by using 1-D basis function on each m-th curved line element expressed as ∂S [67]

$$B_k(u) = u^k, \quad -1 \leqslant u \leqslant 1, \tag{4.14}$$

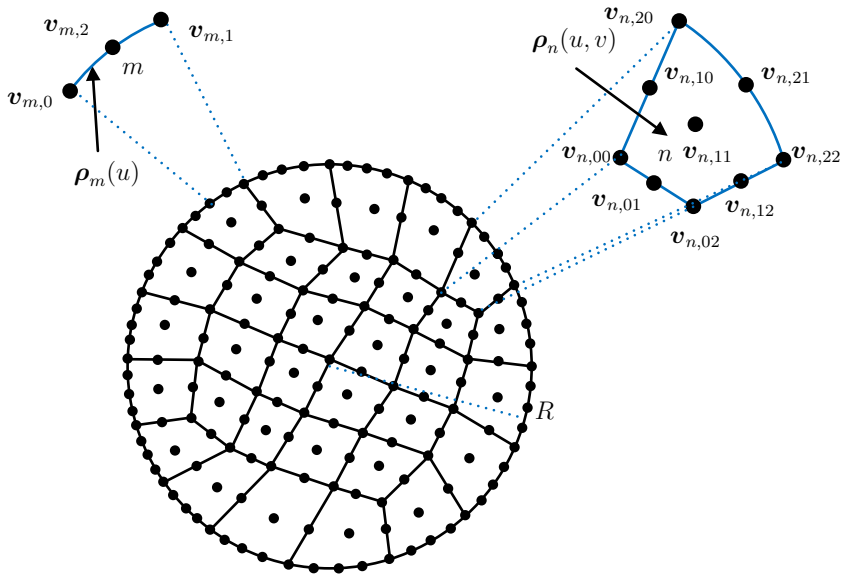

Figure 4.1: Geometrical representation of a circular dielectric cylinder of radius R with second order HO line and quadrilateral elements.

where $k = 0, 1, ..., \Omega - 1$ and Ω is the highest order of current expansion on the 1-D elements. Thus fictitious surface current density $\mathtt{J}_z$ can be written as [67]

$$\mathtt{J}_z(u) \cong \sum_{m=0}^{M-1} \sum_{k=0}^{\Omega-1} \mathcal{I}_{mk} B_k(u), \quad -1 \leqslant u \leqslant 1, \tag{4.15}$$

where k is the order of (4.14), and $\mathcal{I}_{mk}$ is the unknown coefficient of k-th order basis function B_k on the m-th 1-D curved line element.

Discretization of the unknown electric field inside of the scatterer $E_z(\boldsymbol{\rho}_n(u,v))$ on each n-th quadrilateral element is performed using basis functions $b_{j'k'}$ defined as [67]

$$b_{j'k'}(u,v) = u^{j'} v^{k'}, \quad -1 \leqslant u, v \leqslant 1, \tag{4.16}$$

where $j', k' = 0, 1, ..., \Psi - 1$ and Ψ is maximum order of electric field expansion on 2-D HO quadrilateral elements. Thus, the expansion of the electric field E_z inside of

the cross-section of the scatterer over HO basis function $b_{j'k'}$ is the following [67]

$$E_z(u,v) \cong \sum_{n=0}^{N-1}\sum_{j'=0}^{\Psi-1}\sum_{k'=0}^{\Psi-1} \mathrm{i}_{nj'k'}\ b_{j'k'}(u,v), \quad -1 \leqslant u,v \leqslant 1, \tag{4.17}$$

where N is the total number of 2-D HO quadrilateral elements discretizing the scatterer cross-section S, and $\mathrm{i}_{nj'k'}$ is the unknown coefficient of test function $b_{j'k'}$ on n-th higher order quadrilateral element.

4.3.2 Integral Representation of Surface-to-Volume Operator $\mathtt{T}_\epsilon^{S,\partial S}$

We discretize the integral operator $\mathtt{T}_\epsilon^{S,\partial S}$ by using surface basis functions $B_{k''}$ (4.14) on 1-D contour elements and then test with 2-D HO functions $b_{j'k'}$ (4.16) on the 2-D elements discretizing the cross-section. Hence, the matrix elements are defined as the following double inner products

$$\mathcal{Z}_{j'k',k''}^{S_n,\partial S_{m''}} = \langle b_{j'k'}, \langle G_\epsilon, B_{k''}\rangle\rangle = -i\omega\mu_0 \int_{-1}^{1}\int_{-1}^{1} du'dv' b_{j'k'}(u',v')\mathcal{J}_n(u',v') \times \int_{-1}^{1} du'' B_{k''}(u'')\mathfrak{J}_{m''}(u'')G_\epsilon(\boldsymbol{\rho}_n(u',v'),\boldsymbol{\rho}_{m''}(u'')), \tag{4.18}$$

where $\mathfrak{J}_{m''}(u'')$ is the Jacobian of 1-D HO element, and $\mathcal{J}_n(u',v')$ is the Jacobian of n-th 2-D HO quadrilateral element. With proper indexing for total $N\Psi^2$ 2-D HO test functions and total $M\Omega$ 1-D HO basis functions we define the elements of the resultant $(N\Psi^2 \times M\Omega)$ matrix $\bar{\bar{Z}}^{S,\partial S}$ of the discretized operator $\mathtt{T}_\epsilon^{S,\partial S}$ as following

$$Z_{p',q''}^{S,\partial S} = \mathcal{Z}_{j'k',k''}^{S_n,\partial S_{m''}}, \tag{4.19}$$

where $p' = n\Psi^2 + j'\Psi + k'$ and $q'' = m''\Omega + k''$, $n = 0,1,...,N-1$, $j',k' = 0,1,...,\Psi-1$, $m'' = 0,1,...,M-1$, and $k'' = 0,1,...,\Omega-1$.

4.3.3 Integral Representation of Volume-to-Surface Operator $\mathtt{T}_0^{\partial S,S}$

We discretize the integral operator $\mathtt{T}_0^{\partial S,S}$ by using 2-D HO basis functions $b_{j'k'}$ (4.16) in the surface and then test with 1-D HO test functions B_k (4.14). The matrix elements are defined as the double inner products

$$\mathcal{Z}_{k,j'k'}^{\partial S_m,S_n} = \langle B_k, \langle G_0, b_{j'k'} \rangle \rangle = k_0^2(\epsilon - 1) \int_{-1}^{1} du\ B_k(u) \mathfrak{J}_m(u) \int_{-1}^{1}\int_{-1}^{1} du'dv' b_{j'k'}(u',v') \times\ \mathcal{J}_n(u',v') G_0(\boldsymbol{\rho}_m(u), \boldsymbol{\rho}_n(u',v')). \quad (4.20)$$

With proper indexing for total $M\Omega$ 1-D HO basis functions on the surface and all of the $N\Psi^2$ 2-D HO test functions, we define the elements of the resultant $(M\Omega \times N\Psi^2)$ matrix $\bar{\bar{Z}}^{\partial S,S}$ of the operator $\mathtt{T}_0^{\partial S,S}$ as

$$Z_{q,p'}^{\partial S,S} = \mathcal{Z}_{k,j'k'}^{\partial S_m,S_n}, \quad (4.21)$$

where $q = m\Omega + k$, $p' = n\Psi^2 + j'\Psi + k'$ and, $m = 0, 1, ..., M-1$, $k = 0, 1, ..., \Omega - 1$, $n = 0, 1, ..., N-1$, and $j', k' = 0, 1, ..., \Psi - 1$.

4.3.4 Integral Representation of Surface-to-Surface Operator $\mathtt{T}_\epsilon^{\partial S,\partial S}$

The discritized form of the integral operator $\mathtt{T}_\epsilon^{\partial S,\partial S}$ is the scattered field produced by 1-D HO basis functions $B_{k''}$ tested by 1-D HO test functions B_k (4.14). The matrix elements are defined as the following double inner products

$$\mathcal{Z}_{k,k''}^{\partial S_m,\partial S_{m''}} = \langle B_k, \langle G_\epsilon, B_{k''} \rangle \rangle = -i\omega\mu_0 \int_{-1}^{1} du\ B_k(u) \mathfrak{J}_m(u) \times \int_{-1}^{1} du'' B_{k''}(u'') \mathfrak{J}_{m''}(u'')\ G_\epsilon(\boldsymbol{\rho}_m(u), \boldsymbol{\rho}_{m''}(u'')). \quad (4.22)$$

With proper indexing for total $M\Omega$ 1-D HO basis functions (4.14), we define the elements of the resultant $(M\Omega \times M\Omega)$ matrix $\bar{\bar{Z}}^{\partial S,\partial S}$ of the operator $\mathtt{T}_{\epsilon}^{\partial S,\partial S}$ as

$$Z_{q,q''}^{\partial S,\partial S} = \mathcal{Z}_{k,k''}^{\partial S_m,\partial S_{m''}}, \tag{4.23}$$

where $q = m\Omega + k$, $q'' = m''\Omega + k''$, $k, k'' = 0, 1, ..., \Omega - 1$, and $m, m'' = 0, 1, ..., M - 1$.

4.3.5 Integral Representation of $E_z^{\mathbf{inc}}$

The discritized form of the excitation E_z^{inc} is calculated by testing the incident electric field with 1-D higher order test functions (4.14). Each element to fill right hand side vector are defined as

$$\mathcal{V}_{m,k} = \langle B_k, E_z^{\text{inc}} \rangle = \int_{-1}^{1} du\ B_k(u)\mathfrak{J}_m(u)\ E_z^{\text{inc}}(\boldsymbol{\rho}_m(u)). \tag{4.24}$$

Resultant vector $\bar{V}$ of the right hand side is filled by the elements

$$\bar{V}_q = \mathcal{V}_{m,k}, \tag{4.25}$$

where $q = m\Omega + k$, $m = 0, 1, ..., M - 1$ and $k = 0, 1, ..., \Omega - 1$. Once all the matrices regarding operators $\mathtt{T}_{\epsilon}^{S,\partial S}$, $\mathtt{T}_{0}^{\partial S,S}$, $\mathtt{T}_{\epsilon}^{\partial S,\partial S}$, and incident field E_z^{inc} are filled, they create a SLAE with respect to vector of unknown coefficients $\bar{I}$ so that we can compute the surface current density(4.15) as

$$\left(\bar{\bar{Z}}^{\partial S,\partial S} + \bar{\bar{Z}}^{\partial S,S} \cdot \bar{\bar{\Gamma}}^{-1} \cdot \bar{\bar{Z}}^{S,\partial S}\right) \cdot \bar{I} = \bar{V}. \tag{4.26}$$

In (4.26), the elements of Gram matrix $\bar{\bar{\Gamma}}$ are defined as

$$\Gamma_{p,p'}(j,k,j',k') = \int_{-1}^{1}\int_{-1}^{1} du\ dv \mathcal{J}_n(u,v) u^j v^k u^{j'} v^{k'}, \tag{4.27}$$

where $p = n\Psi^2 + j\Psi + k$, $p' = n'\Psi^2 + j'\Psi + k'$, $n, n' = 0, 1, ..., N - 1$, $j, j' = 0, 1, ..., \Psi - 1$ and $k, k' = 0, 1, ..., \Psi - 1$.

4.3.6 Field Inside the Scatterer

After solving the system of linear algebraic equations and finding the vector of unknown coefficients $\bar{I}$, the vector of unknown coefficients $\bar{\mathrm{i}}$ of (4.17) are calculated as

$$\bar{\mathrm{i}} = i\omega\mu_0 \bar{\bar{\Gamma}}^{-1} \cdot \bar{\bar{Z}}^{S,\partial S} \cdot \bar{I}, \tag{4.28}$$

where $\bar{\mathrm{i}}$ is the $(N\Psi^2 \times 1)$ vector of coefficients in expansion of the volumetric polarization current (4.17).

Subsequently, the total electric field inside n-th quadrilateral patch is calculated as

$$E_{z,n}(u,v) \cong \sum_{j'=0}^{\Psi-1} \sum_{k'=0}^{\Psi-1} \mathrm{i}_{n\Psi^2+j'\Psi+k'}\ b_{j'k'}(u,v). \tag{4.29}$$

4.4 Numerical Studies

In order to achieve highly accurate scattered electric field by a dielectric object we have used HO-MoM on SVS-EFIE under TM-polarization. To demonstrate robustness of SVS EFIE example of circular dielectric object has been considered. Geometry discretization of the circular dielectric object has been done through Lagrangian type geometry representation. For this particular example, we illuminate the circular dielectric cylinder of radius 1m with incident electric field $E_z^{\mathrm{inc}}(\boldsymbol{\rho}) = e^{-i\boldsymbol{k}\cdot\boldsymbol{\rho}}$ V/m, where $\boldsymbol{k} = k_0\hat{\mathbf{x}}$ and the incidence angle is 180°. The cylinder is discretized with geometrical order 2 ($\chi = 2$) line and quadrilateral elements as shown in Fig. 4.1 and 3rd order HO-MoM solution of SVS-EFIE is applied to get an error controlled solution at frequency 18 MHz. Finally the result is compared with Mie series solution [47]. Fig. 4.2(a) shows the electric field inside the dielectric circular cylinder and Fig. 4.2(b) shows the relative error between SVS-EFIE and Mie series solution [47].

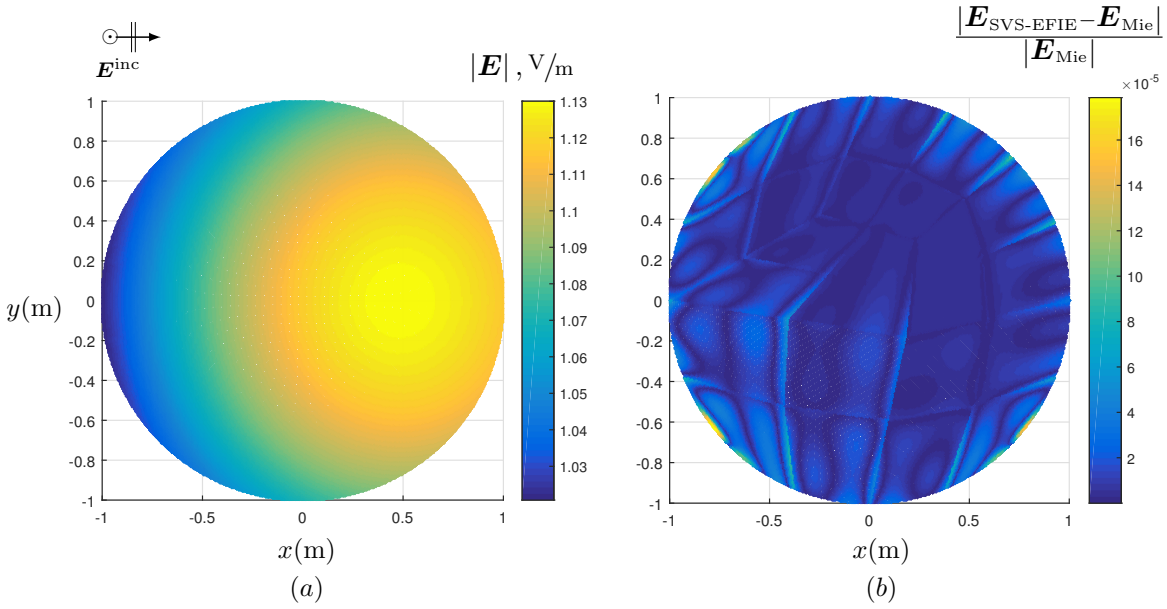

Figure 4.2: (a) Total electric field $|\boldsymbol{E}|$ inside a dielectric cylinder with radius $R = 1$m and permittivity $\epsilon = 2$ for scalar TM case at 18 MHz frequency obtained from the proposed 3rd order ($\Omega = \Psi = 3$) HO MoM solution of the SVS-EFIE (4.6) on the second order meshes consisting of $N = 24$ quadrilaterals and $M = 16$ line elements ($\chi = 2$). (b) The relative error distribution between the 3rd order MoM solution in (a) and Mie series solution [47]. The average relative error is 1.01×10^{-5}.

5

Computational Techniques Required for Achieving Desired Accuracy and Efficiency when Solving SVS-EFIE with HO-MOM

5.1 Green's Function of the Cylindrical Cavity

Faraday's and Ampere's laws can be expressed in frequency domain as

$$\boldsymbol{\nabla} \times \boldsymbol{E}(\boldsymbol{r}) = -i\omega\mu \boldsymbol{H}(\boldsymbol{r}), \tag{5.1}$$

$$\boldsymbol{\nabla} \times \boldsymbol{H}(\boldsymbol{r}) = i\omega\epsilon \boldsymbol{E}(\boldsymbol{r}) + \boldsymbol{j}(\boldsymbol{r}). \tag{5.2}$$

If we substitute $\boldsymbol{H}(\boldsymbol{r})$ from (5.1) into (5.2) then we get

$$\boldsymbol{\nabla} \times \boldsymbol{\nabla} \times \boldsymbol{E}(\boldsymbol{r}) = k^2 \boldsymbol{E}(\boldsymbol{r}) - i\omega\mu \boldsymbol{j}(\boldsymbol{r}), \tag{5.3}$$

where k is the wave number of the object. By using vector identity $\boldsymbol{\nabla} \times \boldsymbol{\nabla} \times \boldsymbol{E}(\boldsymbol{r}) = -\nabla^2 \boldsymbol{E}(\boldsymbol{r}) + \boldsymbol{\nabla}(\boldsymbol{\nabla} \cdot \boldsymbol{E}(\boldsymbol{r}))$, equation (5.3) becomes

$$\nabla^2 \boldsymbol{E}(\boldsymbol{r}) + k^2 \boldsymbol{E}(\boldsymbol{r}) = \boldsymbol{\nabla}(\boldsymbol{\nabla} \cdot \boldsymbol{E}(\boldsymbol{r})) + i\omega\mu \boldsymbol{j}(\boldsymbol{r}). \tag{5.4}$$

If we assume a source free region then $\boldsymbol{j}(\boldsymbol{r}) = 0$ and for a source free region by using Gauss law we can write $\boldsymbol{\nabla} \cdot \boldsymbol{E}(\boldsymbol{r}) = 0$. Electric field inside a source free object is governed by the following homogeneous vector Helmholtz equation as

$$\nabla^2 \boldsymbol{E}(\boldsymbol{r}) + k^2 \boldsymbol{E}(\boldsymbol{r}) = 0, \boldsymbol{r} \in S. \tag{5.5}$$

The vector Helmholtz equation converts into scalar Helmholtz equation under conditions of TM-polarization as

$$\nabla^2 E_z^0(x, y) + k^2 E_z^0(x, y) = 0, \ (x, y) \in S, \tag{5.6}$$

since only z component of the electric field in non zero. Equation (5.6) can be rewritten in the cylindrical coordinates as follows

$$\frac{1}{\rho}\frac{\partial}{\partial \rho}\left(\rho \frac{\partial}{\partial \rho} E_z^0(\rho, \phi)\right) + \frac{1}{\rho^2}\frac{\partial^2}{\partial \phi^2}(E_z^0(\rho, \phi)) + k^2 E_z^0(\rho, \phi) = 0; \ (\rho, \phi) \in S. \tag{5.7}$$

Now, $E_z^0(\rho, \phi)$ can be represented with Fourier series as [56]

$$E_z^0(\rho, \phi) = \sum_{n=-\infty}^{\infty} E_{zn}^0(\rho) e^{-in\phi} \tag{5.8}$$

because it is a periodic function over ϕ coordinate. If we plugin equation (5.8) into equation (5.7) we have

$$\sum_{n=-\infty}^{\infty} \left[\frac{1}{\rho}\frac{\partial}{\partial \rho}\left(\rho \frac{\partial}{\partial \rho} E_{zn}^0(\rho)\right) - \frac{n^2}{\rho^2} E_{zn}^0(\rho) + k^2 E_{zn}^0(\rho)\right] e^{-in\phi} = 0. \tag{5.9}$$

Since the series (5.9) is equal to zero for all $\phi \in [0, 2\pi]$, according to property of Fourier series its coefficients must be equal to zero. Hence, for each n we can write (5.9) as

$$\frac{1}{\rho}\frac{\partial}{\partial\rho}\left(\rho\frac{\partial}{\partial\rho}E^0_{zn}(\rho)\right) + \left(k^2 - \frac{n^2}{\rho^2}\right)E^0_{zn}(\rho) = 0. \tag{5.10}$$

Equation (5.10) is the Bessel equation. The only solution of equation (5.10) which is bounded at the region containing the origin is

$$E^0_{zn}(\rho) = D'_n J_n(k\rho), \tag{5.11}$$

where J_n is the Bessel function of the first kind of order n. At low frequencies $k\rho \to 0$ and we can seek solution in the form

$$E^0_{zn}(\rho) = D_n\ \rho^n. \tag{5.12}$$

If we plugin $E^0_{zn}(\rho)$ into equation (5.8) then we have

$$E^0_z(\rho, \phi) = \sum_{n=-\infty}^{\infty} D_n\ \rho^n e^{-in\phi}. \tag{5.13}$$

When the excitation is due to a filament of current (excitation is Dirac delta function), inhomogeneous Helmholtz equation can be written in cylindrical coordinates as

$$\frac{1}{\rho}\frac{\partial}{\partial\rho}\left(\rho\frac{\partial}{\partial\rho}E^\delta_z(\rho,\phi,\rho',\phi')\right) + \frac{1}{\rho^2}\frac{\partial^2}{\partial\phi^2}(E^\delta_z(\rho,\phi,\rho',\phi')) + k^2E^\delta_z(\rho,\phi,\rho',\phi') = -\frac{1}{\rho}\delta(\rho-\rho')\delta(\phi-\phi'), \tag{5.14}$$

where $(\rho, \phi, \rho', \phi') \in S$. Since $E^\delta_z(\rho, \phi, \rho', \phi')$ is 2π-periodic over ϕ it can be represented with Fourier series as [56]

$$E^\delta_z(\rho,\phi,\rho',\phi') = \sum_{n=-\infty}^{\infty} E^\delta_{zn}(\rho,\rho',\phi')e^{-in\phi}. \tag{5.15}$$

The Fourier series expansion is defined for a periodic function over ϕ coordinate can be written as

$$f(\phi) = \sum_{n=-\infty}^{\infty} \beta_n e^{-in\phi}, \tag{5.16}$$

where

$$\beta_n = \langle f(\phi), e^{in\phi} \rangle = \frac{1}{2\pi} \int_0^{2\pi} f(\phi) e^{in\phi} d\phi. \tag{5.17}$$

If $f(\phi) = \delta(\phi - \phi')$ according to equation (5.16) we can write

$$\delta(\phi - \phi') = \sum_{-\infty}^{\infty} \beta_n^{\delta} e^{-in\phi}, \tag{5.18}$$

where

$$\beta_n^{\delta} = \langle \delta(\phi - \phi'), e^{in\phi} \rangle = \frac{1}{2\pi} \int_0^{2\pi} \delta(\phi - \phi') e^{in\phi} d\phi. \tag{5.19}$$

By using shifting property of delta function we can write

$$\beta_n^{\delta} = \frac{1}{2\pi} \int_0^{2\pi} \delta(\phi - \phi') e^{in\phi} d\phi = \frac{e^{in\phi'}}{2\pi}. \tag{5.20}$$

Now we will substitute β_n^{δ} (5.20) into (5.18) then we get

$$\delta(\phi - \phi') = \sum_{-\infty}^{\infty} \frac{e^{in\phi'}}{2\pi} e^{-in\phi}. \tag{5.21}$$

If we plugin equation (5.21) and (5.15) into equation (5.14) then by using property of Fourier series we can express the Bessel equation for scalar TM mode for Dirac delta function excitation as follows

$$\frac{1}{\rho} \frac{\partial}{\partial \rho} \left(\rho \frac{\partial}{\partial \rho} E_{zn}^{\delta}(\rho, \rho', \phi') \right) + \left(k^2 - \frac{n^2}{\rho^2} \right) E_{zn}^{\delta}(\rho, \rho', \phi') = \frac{-\delta(\rho - \rho') e^{in\phi'}}{2\pi\rho}. \tag{5.22}$$

Solution of equation (5.22) is

$$E^{\delta}_{zn}(\rho,\rho',\phi') = e^{-in\phi'}\begin{cases} J_n(k\rho')H^{(2)}_n(k\rho); & \rho>\rho', \\ J_n(k\rho)H^{(2)}_n(k\rho'); & \rho<\rho', \end{cases} \tag{5.23}$$

where $H^{(2)}_n$ is the Hankel function of the second kind and order n and J_n is the Bessel function of order n. Substituting (5.23) in (5.15) and using addition theorem [14] we get

$$E^{\delta}_{z}(\rho,\phi,\rho',\phi') = \sum_{n=-\infty}^{\infty} e^{in(\phi-\phi')}\begin{cases} J_n(k\rho')H^{(1)}_n(k\rho); & \rho>\rho' \\ J_n(k\rho)H^{(1)}_n(k\rho'); & \rho<\rho' \end{cases} = -\frac{i}{4}H^{(2)}_0(k|\rho-\rho'|), \tag{5.24}$$

where $H^{(1)}_n$ is the Hankel function of the first kind and order n and $H^{(2)}_0$ is the Hankel function of the second kind and order zero. For small arguments when $k\rho \to 0$ and $k\rho' \to 0$ we can express $H^{(2)}_0(k|\rho-\rho'|)$ as [61]

$$H^{(2)}_0(k|\rho-\rho'|) \cong \frac{2}{\pi i}\begin{cases} \ln(\rho), \rho>\rho' \\ \ln(\rho'), \rho<\rho' \end{cases} + \sum_{n=1}^{\infty} 2C_n\cos[n(\phi-\phi')]\begin{cases} {(\rho')^n}/{\rho^n}, \rho>\rho' \\ {\rho^n}/{(\rho')^n}, \rho<\rho' \end{cases} \tag{5.25}$$

where $C_n = -1/(n\pi i), n = 1, 2, ...\infty$. Since the expression in the right hand side of (5.25) is equal to $2/(\pi i)\ln|\boldsymbol{\rho}-\boldsymbol{\rho'}|$, the field $E^{\delta}_z(\rho,\phi,\rho',\phi')$ is nothing but the static free space Green's function $G_0(\boldsymbol{\rho},\boldsymbol{\rho'})$ as [61]

$$E^{\delta}_z(\rho,\phi,\rho',\phi') = G_0(\boldsymbol{\rho},\boldsymbol{\rho'}) = -\frac{1}{2\pi}\ln|\boldsymbol{\rho}-\boldsymbol{\rho'}|. \tag{5.26}$$

The z component of electric field E_z can then be represented as a superposition of the homogenous solution and inhomogeneous solution as follows

$$E_{zn} = E^{0}_{zn} + E^{\delta}_{zn}. \tag{5.27}$$

In order to construct the Green's function of cylindrical cavity with radius R_0 out of the field expression (5.27), we impose boundary condition $E_{zn} = 0$ on (5.27) at

observation point $\rho = R_0$. This relates coefficients D_n in (5.13) to the coefficients C_n in (5.25), as

$$D_n = \begin{cases} (iC_n\ (\rho')^n)/(4(R_0)^{2n}); & n \neq 0, \\ (1/2\pi)\ln(R_0); & n = 0 \end{cases} \tag{5.28}$$

yielding sought closed form expression for the Green's function of cylindrical cavity by using superposition of inhomogeneous solution (5.26) and homogenous solution (5.13) as [59]

$$E_z(\boldsymbol{\rho}, \boldsymbol{\rho}') = E_z^{\delta} + E_z^0 = G_0(\boldsymbol{\rho}, \boldsymbol{\rho}') + \frac{\ln(R_0)}{2\pi} - \frac{1}{2\pi}\sum_{n=1}^{\infty} \frac{|\boldsymbol{\rho}|^n |\boldsymbol{\rho}'|^n}{nR_0^{2n}} \cos\left(n(\phi - \phi')\right), \tag{5.29}$$

where ϕ and ϕ' are the polar co-ordinate angles correspond to position vector $\boldsymbol{\rho}$ and $\boldsymbol{\rho'}$, respectively.

5.1.1 Numerical Evaluation

We consider a cylindrical cavity with radius $R_0 = 1$m and source point located at $\rho' = 0.5$m, $\phi' = 0.25\pi$. The magnitude of electric field or Green's function of cylindrical cavity $E_z(\boldsymbol{\rho}, \boldsymbol{\rho}')$ (5.29) produced by that point source is shown in Fig. 5.1. One can observe that electric field goes to zero at the boundary according to the enforced boundary condition at $R_0 = 1$m.

When we try to compare the result of SVS EFIE [36] HO-MOM with COMSOL [51] we have to keep the fact in mind that COMSOL is a finite element solver which truncates its mesh at a certain distance away around the object and applies boundary condition there. We have to impose the same boundary condition to HO-MoM through the above derivation of Green's function of cylindrical cavity $E_z(\boldsymbol{\rho}, \boldsymbol{\rho}')$ (5.29) instead of free space Green's function $G_0(\boldsymbol{\rho}, \boldsymbol{\rho}') = -\frac{1}{2\pi}\ln(|\boldsymbol{\rho} - \boldsymbol{\rho}'|)$ in order to obtain the fields matching with controlled precision those of HO-FEM.

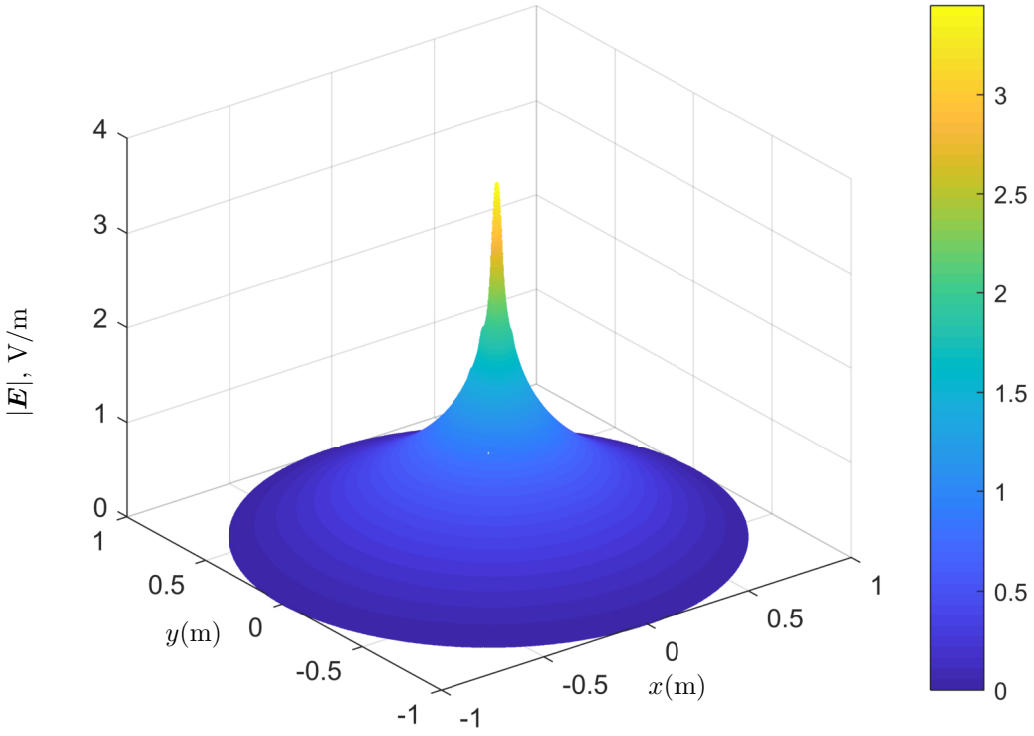

Figure 5.1: Volumetric distribution of $|\boldsymbol{E}|$ TM polarized in circular cylinder with radius $R_0 = 1\text{m}$.

5.2 Study of Skin Effect on a Circular Conductor

At low frequencies the current flows throughout the entire conductor cross-section. However, when we increase the frequency, the current accumulates near the surface of the conductor and the current in the middle region of the conductor becomes negligible. This phenomena is called skin effect [48]. The explanation for this effect is the following. When time varying magnetic field is applied to a conducting object it creates electro motive force within it, which then creates eddy currents flowing in the object of such directions that will minimize the overall magnetic field [48]. As a result, the intensity of the time-harmonic fields in metal conductors attenuates exponentially away from their boundaries [2]. Because of the skin-effect, at higher frequencies we can calculate the impedance of a conductor by meshing only a small region near its

boundary where the most of the current is flowing [48]. To demonstrate, instead of a circular conductor we can consider a circular shell as shown in Fig. 5.2. The outer radius R is same as the radius of original conductor and the inner radius R_L. The R_L will depend on the following expression while calculating the net current I in the conductor according to our desired accuracy I_{err}

$$I_{\text{err}} = \frac{|I_{\text{circle}} - I_{\text{shell}}|}{|I_{\text{circle}}|}, \tag{5.30}$$

where

$$I_{\text{circle}} = \iint_{S_{\text{circle}}} j_z ds = 2\pi \int_0^R j_z(k_\sigma \rho)\rho d\rho, \tag{5.31}$$

$$I_{\text{shell}} = \iint_{S_{\text{shell}}} j_z ds = 2\pi \int_{R_L}^R j_z(k_\sigma \rho)\rho d\rho. \tag{5.32}$$

In (5.31)-(5.32), k_σ is the wave number of the conductor and I_{err} is the relative error between total current I_{circle} flowing through the circular conductor, I_{shell} total current flowing through the shell, and j_z is the volumetric current distribution on the conductor.

Another important factor to notice in the SVS-EFIE formulation is that the Green's function of conducting media $G_\sigma(\boldsymbol{\rho}', \boldsymbol{\rho}'') = -iH_0^{(2)}(k_\sigma|\boldsymbol{\rho}' - \boldsymbol{\rho}''|)/4$ decays very rapidly when we go to high frequencies because of the skin effect. So for gaining computational efficiency we can make the integrals associated with HO-MOM solution of SVS EFIE (3.5) zero if the distance between the source $\boldsymbol{\rho}''$ and observation point $\boldsymbol{\rho}'$ is greater than certain distance. For example, if we want relative error in the field or current computation to be 10^{-6}, we make the integrals associated with HO-MOM solution of SVS EFIE (3.5) zero, when $|\boldsymbol{\rho}' - \boldsymbol{\rho}''| < [-\ln(10^{-6})]\delta$ [2].

To demonstrate this numerically, consider a circular aluminium shell shown in Fig. 5.2 with outer radius $R = 0.025$ m. Using (5.30) we can find that, if we want $I_{\text{err}} = 10^{-6}$ at $f = 1$ MHz, then inner radius R_L has to be at most 0.023 m. Table 5.1 shows the relative error in p.u.l. resistance R and inductance L between the HO-MoM solution of SVS-EFIE and analytical solution for 1 MHz frequency.

Table 5.1: Values of p.u.l. resistance R and inductance L computed using 2nd order MoM solution ($\Omega = \Psi = 2$) of SVS-EFIE (3.5) with $M = 20$ contour and and $N = 40$ volume elements for circular shell conductor with outer radius $R = 0.025$ m and inner radius $R_L = 0.023$m at frequency $f = 1$ MHz. Analytical solutions are provided for reference.

	R(mΩ/m)	L(μH/m)
Analytical Circle	2.120595499681E-03	7.38112825016E-07
Analytical Shell	2.120595286164E-03	7.381128250226E-07
HO-MoM SVS-EFIE (Circular shell)	2.241676594124E-03	7.37836621569E-07
Relative Error in SVS-EFIE	~ 0.01	~ 0.0001

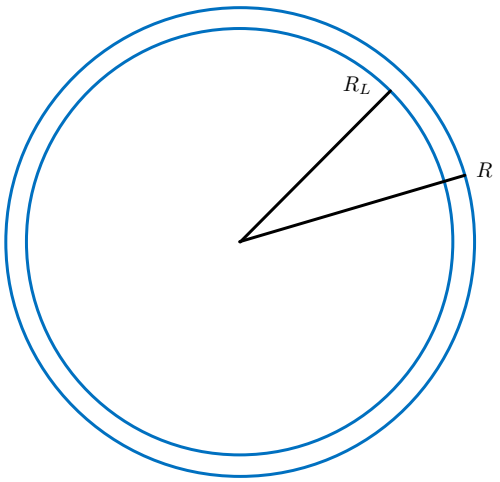

Figure 5.2: Circular shell with inner radius $R_L = 0.023$ m and outer radius $R = 0.025$ m.

5.3 Logarithmic Singularity and Near-Singularity Extraction from 1-D Integrals Over HO Curved Line Elements in HO-MoM Solution of SVS-EFIE

When solving SVS-EFIE with MoM singular and near-singular integrals are encountered when observation point is near or overlaps with the source element. These integrals need to be handled with care if we want an error controlled solution. In this situation the logarithmic function varies rapidly. As a result, one needs to use quadrature rules of high orders to ensure that the integral is computed accurately. Common approach to circumvent this issue is to subtract analytically integrable singular portion of the integrand and then add it's contribution in the form of a closed-form integration result. Such analytical integral in closed form for ln function can be found in [54]. This process is straight forward for a first order elements.

When we are dealing with HO line element it becomes more difficult. To apply singularity extraction to HO line element we have to create a tangential line at the observation point defined by parametric coordinate u as shown in Fig. 5.3. This coordinate u corresponds to the closest location on the source HO element to the observation point. Subsequently, each point from the HO element is projected onto the tangential 1st order element (straight line) and the conventional singularity procedure is applied as

$$\mathcal{I}(\boldsymbol{\rho}) = \int_{-1}^{1} du''[\,\ln(|\boldsymbol{\rho}-\boldsymbol{\rho}''(u'')|)f(u'')\mathfrak{J}(u'') - \ln(|\boldsymbol{\rho}-\boldsymbol{\rho}_t''(u,u'')|)f(u)\mathfrak{J}(u)\,]+ \\ f(u)\mathfrak{J}(u)/\mathfrak{J}_t(u)\int_{-1}^{1} du''\ln(|\boldsymbol{\rho}-\boldsymbol{\rho}_t''(u,u'')|)\mathfrak{J}_t(u)\,, \quad (5.33)$$

where f is a scalar function which is monomial basis function in the case of MoM, $\boldsymbol{\rho}$ is the position vector for the observation point, $\boldsymbol{\rho}''$ is the position vector for the source point, $\boldsymbol{\rho}_t''(u,u'') = \big([\boldsymbol{\rho}''(u'')\cdot\hat{\mathbf{t}}(u)]\hat{\mathbf{t}}(u)+[\boldsymbol{\rho}''(u)\cdot\hat{\mathbf{n}}(u)]\hat{\mathbf{n}}(u)\big)$ is the position vector on the tangential straight line created at the point on HO element closest to the observation

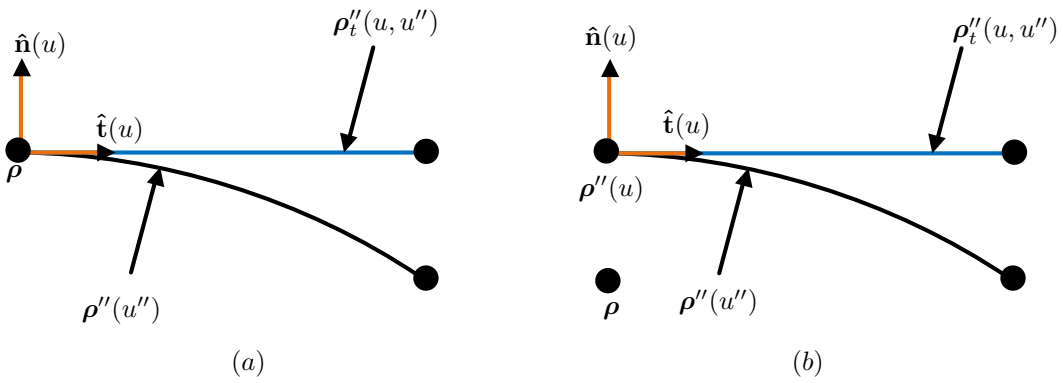

Figure 5.3: (a) Singularity and (b) near-singularity extraction on 1-D HO curved element.

point and having parametric location u, $\hat{\mathbf{n}}(u)$ is the unit normal vector at location u, $\hat{\mathbf{t}}(u)$ is unit tangent vector at location u defined as $\hat{\mathbf{t}}(u) = {}^{\boldsymbol{a}(u)}/_{|\boldsymbol{a}(u)|}$, $\boldsymbol{a}(u) = \frac{\partial}{\partial u}(\boldsymbol{\rho}(u))$, $\mathfrak{J}(u'')$ is Jacobian of the curvilinear line defined as $\mathfrak{J}(u'') = |\boldsymbol{a}(u'')|$, and $\mathfrak{J}_t(u) = \left|\frac{\partial}{\partial u''}(\boldsymbol{\rho}_t''(u,u''))\right|$ is the Jacobian of the projected straight line created at location u. Singular part is extracted in the first integral of (5.33). The second integral (5.33) over straight line is analytically integrable [54].

6

Conclusions and Future Work

6.1 Conclusions

In this thesis HO-MoM solution of SVS-EFIE has been demonstrated for error-controllable extraction of p.u.l. resistance and inductance in arbitrary shaped MTLs. Numerical results are provided for complex sector shaped cable and compared with HO-FEM from COMSOL [51] for frequencies 60Hz and 1KHz. In order to control the error of the proposed HO-MoM solution of the SVS-EFIE compared to the reference HO-FEM solution, the Green's function of cylindrical cavity is derived and introduced into the SVS-EFIE.

Skin effect is studied and p.u.l. resistance and inductance values are extracted for single circular shell to demonstrate complexity reduction in the HO-MoM solution of SVS-EFIE through elimination of the internal volume of the conductor with negligible level of the current.

HO-MoM solution of SVS-EFIE is also demonstrated for solution of the 2-D scattering problem on a circular dielectric object under TM-polarization. Error controllability of the numerical solution demonstrates rigorous nature of the SVS-EFIE.

Singularity extraction approach is used to control the error in HO-MoM integrals when observation point is on the source element or projects on it.

6.2 Future Work

- By the end of this work C++ implementation for p.u.l. inductance and resistance extraction remains inefficient. Considerable speed up can be achieved if the part of the code handling geometry related operation on HO elements is optimized.

- RL extraction has been done when the background is free space. In the future free space Green's function can be replaced by multilayered Green's function. This will enable calculation of p.u.l. resistance and inductance for conductors in the presence of the multilayered media [37].

- At high frequencies the skin effect phenomena can be utilized to confine the region of the sought current to the thin layer near the conductor surface. The rest of the conductor volume can be eliminated. This property can be applied to arbitrary shaped cables including the sector shaped cable considered in this work. As a result, computational cost will reduce significantly.

- The C++ implementation of the code for RL extraction is sequential at present. It can be parallelized for shared memory [58] and/or distributed memory multiprocessor machines resulting in substantial speed up of the computations.

A

Study of Higher Order Behaviour of Commercial Solver COMSOL for Current Flow Modelling

COMSOL is a multi-physics software package based on Finite Element Method (FEM). FEM solves partial differential equation with a boundary condition. COMSOL can be used to compute volumetric current distribution for conductors of arbitrary shape which can be integrated to find admittance and impedance matrices. For solving current flow problem in COMSOL first we need to build the geometry of the object and select the material for each region. Finally we need to select magnetic and electric fields (mef) interface under AC/DC branch highlighted in Fig. A.1. After that we have to mesh the object, excite the object with external current density $\boldsymbol{J}_e$ which is in our case 1V/m and run the simulation [51]. COMSOL solves equations shown in Fig. A.1 which are under magnetic and electric fields (mef) interface by using FEM. COMSOL truncates the mesh after certain radius away from the object and applies the boundary condition $\hat{\mathbf{n}} \times \boldsymbol{A} = 0$ under magnetic insulation option highlighted in Fig. A.2 [51] that means at that radius tangential component of the vector potential $\boldsymbol{A}$ is forced to zero. We simulated coaxial cable under these settings to obtain p.u.l. resistance and inductance at 60 Hz and it was compared with analytic solution [69] and relative error between COMSOL and analytic solution is

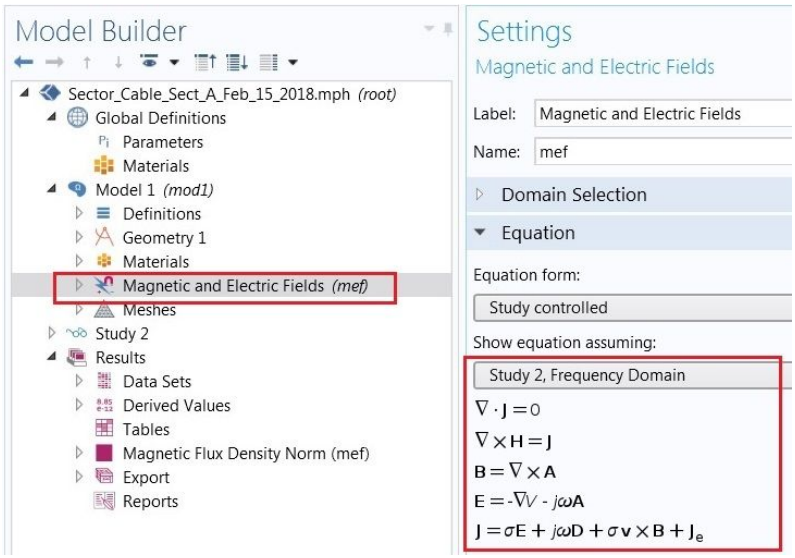

Figure A.1: Equations used by COMSOL under magnetic and electric fields (mef) interface.

shown in Fig. A.4 which was obtained by varying the order of solution in COMSOL by changing the discretization into linear (1st order), quadratic (2nd order) and cubic (3rd order) shown in Fig. A.3 and total number of volume elements. Fig. A.4 clearly shows $O(h^p)$ error convergence [51].

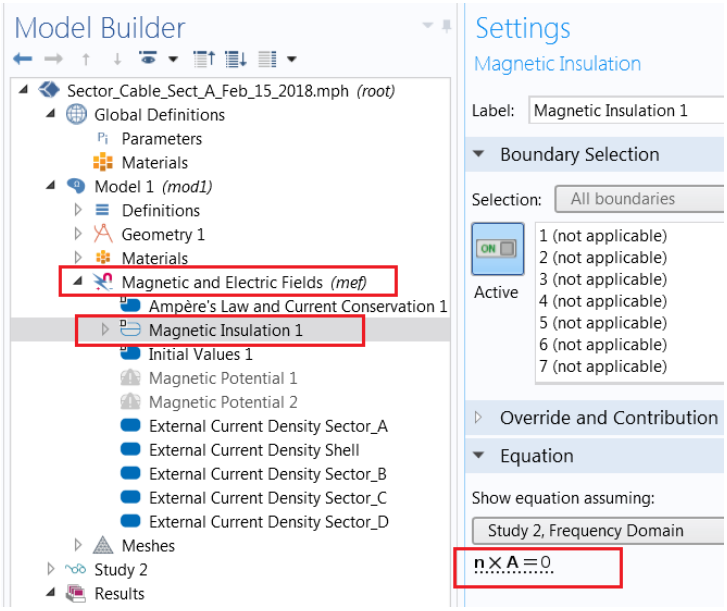

Figure A.2: Boundary condition used by COMSOL under magnetic and electric fields (mef) interface.

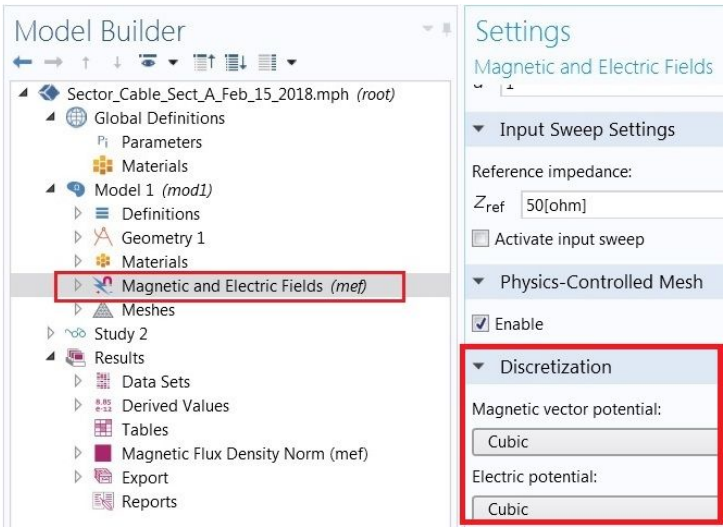

Figure A.3: Changing order of FEM solution under Discretization in COMSOL.

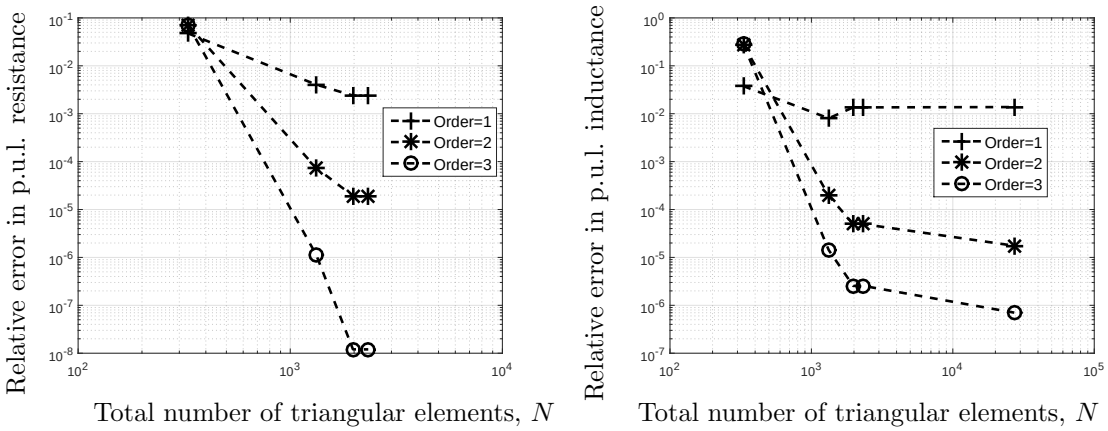

Figure A.4: Relative error in p.u.l. resistance (a) and inductance (b) of a co-axial cable compared between HO-COMSOL [51] and analytic solution [69] by changing order of solution and total volume elements.

References

[1] B. Young, *Digital Signal Integrity: Modeling and Simulation with Interconnects and Packages*. Upper Saddle River, NJ: Prentice Hall, Oct. 2000.

[2] M. Shafieipour, H. M. J. S. P. DeSilva, K. K. M. A. Kariyawasam, A. Menshov, and V. Okhmatovski, "Fast computation of the electrical parameters of sector-shaped cables using single-source integral equation and 2D moment-method discretization," in *Int. Conf. Power Syst. Transients,* Seoul, South Korea, Jun. 2017, pp. 1–6.

[3] A. Menshov, V. Okhmatovski, H. M. J. S. P. DeSilva, K. K. M. A. Kariyawasam, and J. E. Nordstrom, "Modeling of arbitrary shaped cables using novel single source integral equation formulation," in *Int. Conf. Power Syst. Transients*, Cavtat, Croatia, Jun. 2015, pp. 1–6.

[4] Anton Menshov, "Novel Single-Source Surface Integral Equations for Scattering on 2-D Penetrable Cylinders and Current Flow Modelling in 2-D and 3-D Conductors," *M.Sc. Thesis*, Dept. Electr. Comput. Eng., Univ. Manitoba, Winnipeg, Canada, 2014.

[5] J. - M. Jin, *The Finite Element Method in Electromagnetics,* 2nd ed. New York: Wiley, 2002.

[6] Matthew N.O. Sadiku, *Numerical techniques in electromagnetics,* CRC Press LLC, 2001.

[7] A. Peterson, S. Ray, and R. Mittra, *Computational Methods for Electromagnetics,* New York: IEEE Press, 1998.

[8] N. Morita, N. Kumagai, and J. R. Mautz, *Integral Equation Methods for Electromagnetics,* Boston: Artech House, 1990.

[9] Roger F. Harrington, *Field Computation by Moment Methods,* Wiley-IEEE Press, April 1993.

[10] Roger F. Harrington, "Boundary integral formulations for homogeneous material bodies," *Journal of Electromagnetic Waves and Applications,* vol. 3, no. 1, pp. 1–15, January 1989.

[11] R. Mittra, Ed., *Computer Techniques for Electromagnetics,* New York: Hemisphere, 1987.

[12] A. Kishk and L. Shafai, "Different formulations for numerical solution of single or multibodies of revolution with mixed boundary conditions," *IEEE Trans. Antennas Propag.,* vol. 34, no. 5, pp. 666–673, May 1986.

[13] C. Müller, *Foundations of the Mathematical Theory of Electromagnetic Waves,* New York: Springer-Verlag, 1969.

[14] W. C. Chew, *Waves and Field in Inhomogeneous Media,* IEEE Press, 1995.

[15] D. Swatek, "Investigation of single-source surface integral equation for electromagnetic wave scattering by dielectric bodies," *Ph.D. Thesis*, Dept. Electr. Comput. Eng., Univ. Manitoba, Winnipeg, Canada, 1999. [Online]. Available: http://hdl.handle.net/1993/1699.

[16] Jian-Ming Jin, *Theory and Computation of Electromagnetic Fields,* Wiley-IEEE Press, 2010.

[17] J. R. Mautz and R. F. Harrington, "An E-field solution for a conducting surface small or comparable to the wavelength," *IEEE Transactions on Antennas and Propag.,* vol. 32, pp. 330–339, 1984.

[18] Zhi Guo Qian and Weng Cho Chew, "An augmented electric field integral equation for low frequency electromagnetic analysis," *2008 IEEE Antennas and Propagation Society International Symposium.*

[19] J. R. Mautz and R. F. Harrington, "H-field, E-field, and combined- field solutions for conducting bodies of revolution," *Arch. Elek. Übertragung.,* vol. 32, pp. 157–164, 1978.

[20] S. Ramo, J. R. Whinnery, and T. Van Duzer, *Fields and Waves in Communication Electronics*, 2nd ed., New York, Wiley, 1984.

[21] C. R. Paul, *Analysis of Multiconductor Transmission Lines.* New York: Wiley-IEEE Press, Oct. 2007.

[22] E. Tancer, "Extraction of parameters for high speed digital interconnects," Ph.D. Dissertation, Dept. Elect. Comput. Eng., The Univ. Texas Austin, Austin, TX, 1995.

[23] U. R. Patel and P. Triverio, "Skin effect modeling in conductors of arbitrary shape through a surface admittance operator and the contour integral method," *IEEE Trans. Microw. Theory Techn.*, vol. 64, no. 9, pp. 2708–2717, Sep. 2016.

[24] R. Lucas and S. Talukdar, "Advances in finite element techniques for calculating cable resistances and inductances," *IEEE Trans. Power App. Syst*, vol. PAS-97, no. 3, pp. 875–883, May 1978.

[25] A. Menshov and V. Okhmatovski, "New single-source surface integral equations for scattering on penetrable cylinders and current flow modeling in 2-D conductors," *IEEE Trans. Microw. Theory Techn.*, vol. 61, no. 1, pp. 341–350, Jan. 2013.

[26] Daniel Fleisch, *A Student's Guide to Maxwell's Equations,* Cambridge University Press, 2008.

[27] Robert E. Collin, *Field Theory of Guided Waves,* Wiley-IEEE Press, 1990.

[28] K. K. M. A. Kariyawasam, A. M. Gole, B. Kordi, and H. M J. S P. DeSilva, "Accurate electromagnetic transient modelling of sector-shaped cables," in *Int. Conf. Power Syst. Transients (IPST 2011)*, Delft, the Netherlands, Jun. 2011, pp. 1–6.

[29] L. M. Wedepohl and D. J. Wilcox, "Transient analysis of underground power-transmission systems. System-model and wave-propagation characteristics" in *Proc. Inst. Elect. Eng.,* vol. 120, no. 2, pp. 253–260, Feb. 1973.

[30] R. D. Graglia and A. F. Peterson, *Higher Order Techniques in Computational Electromagnetics*. Raleigh, NC: SciTech, Mar. 2016.

[31] S. Wandzura,"Fast methods for fast computers," *Workshop Fast Approximate Algorithms*, Center Sci. Computation Math. Modeling, Univ. Maryland, Apr. 19–30, 2004.

[32] I. Jeffrey, J. Aronsson, M. Shafieipour, and V. Okhmatovski, "Error controllable solutions of large-scale problems in electromagnetics: MLFMA-accelerated locally corrected Nyström solutions of CFIE in 3D," *IEEE Antennas Propag. Mag.*, vol. 55, no. 3, pp. 294–308, Jun. 2013.

[33] M. Shafieipour, "Efficient error-controllable high-order electromagnetic modelling of scattering on electrically large targets with the locally corrected Nyström method," Ph.D. Thesis, Dept. Electr. Comput. Eng., Univ. Manitoba, Winnipeg, Canada, 2016.

[34] M. Djordjevic and B. M. Notaros, "Double higher order method of moments for surface integral equation modeling of metallic and dielectric antennas and scatterers," *IEEE Trans. Antennas Propag.*, vol. 52, no. 8, pp. 2118–2128, Aug. 2004.

[35] R. F. Harrington, "Matrix methods for field problems," *Proc. IEEE*, vol. 55, no. 2, pp. 136–149, Feb. 1967.

[36] V. Okhmatovski, A. Menshov, F. L. S. Hosseini, and S. Zheng, "Novel single-source integral equation in electromagnetics," in *URSI Int. Symp. Electromagnetic Theory*, Espoo, Finland, Aug. 2016, pp. 484–487.

[37] S. Zheng, A. Menshov, and V. Okhmatovski, "New single-source surface integral equation for magneto-quasi-static characterization of transmission lines situated in multilayered media," *IEEE Trans. Microw. Theory Techn.*, vol. 64, no. 12, pp. 4341–4351, Dec. 2016.

[38] A. Menshov and V. Okhmatovski, "Novel single-source surface integral equation for broadband RL extraction in 3-D interconnects," in *IEEE 17th Work. Signal Power Integr.*, Paris, France, May 2013, pp. 1–2.

[39] E. Jorgensen, J. L. Volakis, P. Meincke, and O. Breinbjerg, "Higher order hierarchical Legendre basis functions for electromagnetic modeling," *IEEE Trans. Antennas Propag.*, vol. 52, no. 11, pp. 2985–2995, Nov. 2004.

[40] R. D. Graglia, D. R. Wilton, and A. F. Peterson, "Higher order interpolatory vector bases for computational electromagnetics," *IEEE Trans. Antennas Propag.*, vol. 45, no. 3, pp. 329–342, Mar. 1997.

[41] S. M. Wandzura, "Electric current basis functions for curved surfaces," *Electromagnetics*, vol. 12, no. 1, pp. 77–91, Jan. 1992.

[42] E. Jorgensen, J. L. Volakis, P. Meincke, and O. Breinbjerg, "Higher order hierarchical discretization scheme for surface integral equations for layered media," *IEEE Trans. Geosci. Remote Sens.*, vol. 42, no. 4, pp. 764–772, Apr. 2004.

[43] B. Gustavsen, A. Bruaset, J. J. Bremnes, and A. Hassel, "A finite-element approach for calculating electrical parameters of umbilical cables," *IEEE Trans. Power Del.*, vol. 24, no. 4, pp. 2375–2384, Oct. 2009.

[44] F. Sheikh Hosseini Lori, M.S. Hosen, A. Menshov, M. Shafieipour, and V. Okhmatovski, "Accurate transmission lines characterization via higher or-

der moment method solution of novel single-source integral equation," in *IEEE MTT-S Int. Microw. Symp.,* Jun. 2017, pp. 694–696.

[45] S. A. Schelkunoff, "The electromagnetic theory of coaxial transmission lines and cylindrical shields," in *Bell Syst. Tech. J.*, vol. 13, no. 4, pp. 532–579, Oct. 1934.

[46] F. Sheikh Hosseini Lori, M. S. Hosen, M. Shafieipour, A. Menshov, and V. Okhmatovski, "Accurate characterization of coaxial transmission line via higher order moment method solution of novel single-source surface integral equation," in *IEEE 21st Work. Signal Power Integr.*, Lake Maggiore, Italy, May 2017, pp. 1–4.

[47] F. Sheikh Hosseini Lori, "Novel single source integral equation for analysis of electromagnetic scattering by penetrable objects," Ph.D. dissertation, Dept. Electr. Comput. Eng., Univ. Manitoba, Winnipeg, Canada, 2017.

[48] Zoya Popovic and Branko D. Popovic, *Introductory Electromagnetics,* Prentice Hall, Upper Saddle River, New Jersey, Oct 15, 1999.

[49] W. C. Chew, J. - M. Jin, E. Michielssen, and J. Song, (ed.) *Fast and Efficient Algorithms in Computational Electromagnetics,* Norwood: Artech House, 2001.

[50] S. Zheng, A. Menshov, and V. Okhmatovski, "New single-source surface integral equation for magneto-quasi-static characterization of transmission lines situated in multilayered media," *IEEE Trans. Microw. Theory Techn.,* vol. 64, no. 12, pp. 4341-4351, Dec. 2016.

[51] *COMSOL Multiphysics RF Module User's Manual,* COMSOL AB, Stockholm, Sweden, 2016.

[52] F. Sheikh Hosseini Lori, M. S. Hosen, and V. Okhmatovski, "Higher order method of moments solution of the new vector single-source surface integral equation for 2D TE scattering by dielectric objects," *IEEE NEMO'2017,* Sevilla, Spain, May 17-20, 2017,pp. 161-163.

[53] J. Richmond, "Scattering by a dielectric cylinder of arbitrary cross section shape," *IEEE Trans. Antennas Propag.,* vol. 13, no. 3, pp. 334–341, 1965.

[54] D. R. Wilton, S. M. Rao, A. W. Glisson, D. H. Schaubert, O. M. Al-bundak and C. M. Butler, "Potential integrals for uniform and linear source distributions on polygonal and polyhedral domains," *IEEE Trans. Antennas Propag.,* vol. 32, no. 3, pp. 409–418, Mar. 1984.

[55] C. Geuzaine and J. Remacle, "Gmsh: A 3-D finite element mesh generator with built-in pre-and post-processing facilities," *Int. J. Num. Methods in Engineering,* vol. 79, no. 11, pp. 1309–1331, 2009, available: http://geuz.org/gmsh/.

[56] Hyo J. Eom, *Electromagnetic Wave Theory for Boundary-Value Problems: An Advanced Course on Analytical Methods*, Springer, 2004.

[57] Richard C. Fernow, *Principles of Magnetostatics,* Cambridge University Press, 2016.

[58] OpenMP (Jan. 19, 2017). [Online]. Available: http://www.openmp.org/

[59] Farhad Sheikh Hosseini Lori, Mohammad Shakander Hosen Anton Menshov, Mohammad Shafieipour, and Vladimir I. Okhmatovski, "New Higher Order Method of Moments for Accurate Inductance Extraction in Transmission Lines of Complex Cross Section," *IEEE Transactions on Microwave Theory and Techniques,* vol. 65, pp. 5104–5112, 2017.

[60] Jean-Paul Berrut, Lloyd N. Trefethen, "Barycentric Lagrange Interpolation," *Society for Industrial and Applied Mathematics,* vol. 46, no. 3, pp. 501–517, 2004.

[61] M. Abramowitz and I. A. Stegun *Handbook of Mathematical Functions,* New York: Dover, 1965.

[62] Roger A. Horn and Charles R. Johnson, *Matrix Analysis,* Cambridge University Press 1994.

[63] M. F. Catedra, R. F. Torres, J. Basterrechea, E. Cago, *The CG-FFT Method: Application of Signal Processing Techniques to Electromagnetics,* Artech House, 1995.

[64] J. R. Phillips and J. K. White, "A precorrected-FFT method for electrostatic analysis of complicated 3-D structures," *IEEE Trans. Comput.-Aided Des. Integr. Circuits Syst.*, vol. 16, no. 10, pp. 1059–1072, Oct. 1997.

[65] J. Song, Cai-Cheng Lu, Weng Cho Chew, "Multilevel Fast Multipole Algorithm for Electromagnetic Scattering by Large Complex Objects," *IEEE Transactions on Antennas and Propagation,* vol. 45 no. 10, pp. 1488–1493, Oct 1997.

[66] Haobo Yuan, Nan Wang, and Changhong Liang, "Combining the higher order method of moments with geometric modelling by NURBS Surfaces," *IEEE Transactions on Antennas and Propagation,* vol. 57 no. 11, pp. 3558–3563, November 2000.

[67] Branislav M. Notaros, "Higher Order Frequency-Domain Computational Electromagnetics," *IEEE Transactions on Antennas and Propagation,* vol. 56 no. 8, pp. 2251–2276, Aug 2008.

[68] C. Blanc, C. Schlick, "Accurate parametrization of conics by NURBS," *IEEE Computer Graphics and Applications,* vol. 16 no. 6, pp. 64–71, 1996.

[69] S. A. Schelkunoff, "The electromagnetic theory of coaxial transmission lines and cylindrical shields," *Bell Syst. Tech. J.,* vol. 13 no. 4, pp. 532–579, Oct. 1934.